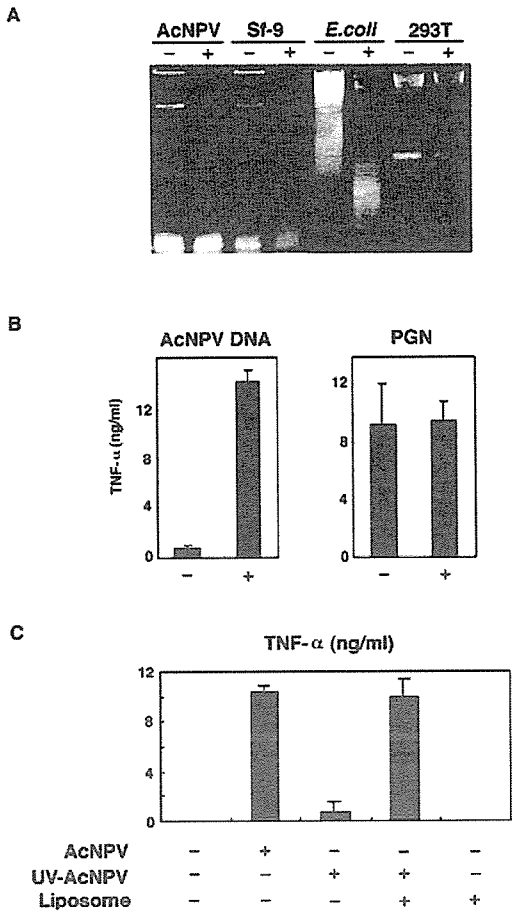

FIG. 5. Activation of mouse macrophage cell line by AcNPV DNA. (A) Methylation status of genomic DNA. Genomic DNAs obtained from AcNPV, Sf-9 cells, *E. coli*, and 293T cells were digested with the methylation-sensitive restriction enzyme HpaII. Undigested (−) and digested (+) samples were analyzed by agarose gel electrophoresis. (B) RAW264.7 cells (10^6 cells/well) were treated with AcNPV DNA (5 μg/ml) or PGN (2.5 μg/ml) in the absence (−) or presence (+) of liposomes for 24 h, and the production of TNF-α in culture supernatants was determined by a sandwich ELISA. Data are shown as means ± SD. (C) Activation of RAW264.7 cells (10^6 cells/well) inoculated with untreated or UV-inactivated AcNPV (5 μg/ml) in the presence or absence of liposomes was assessed by the production of TNF-α in culture supernatants. Data are shown as means ± SD.

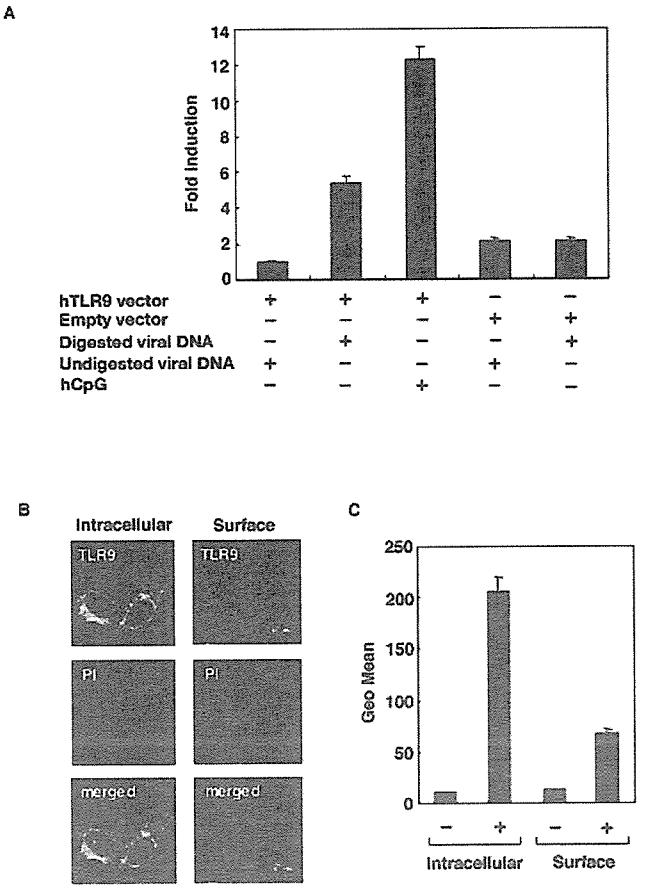

FIG. 6. AcNPV DNA induces NF-κB activation through human TLR9. (A) 293T cells were transfected with an empty or human TLR9 expression vector together with a pELAM luciferase reporter plasmid. Twenty-four hours after transfection, the cells were stimulated with digested or undigested AcNPV DNA (10 μg/ml). hCpG (10 μg/ml) was used as a positive control. The luciferase activity was determined at 24 h posttransfection and expressed as the level of induction compared with that detected in cells transfected with the human TLR9 expression vector alone. Data are shown as means ± SD. (B) Immunofluorescence micrographs of 293T cells transfected with an N-terminal Flag-tagged human TLR9 expression vector and stained with an anti-Flag (M2) monoclonal antibody. The intracellular (left) and cell surface (right) expression of TLR9 is shown. Nuclei were stained with propidium iodide (PI). Samples were observed by confocal microscopy. (C) The surface and intracellular expression of human TLR9 in 293T cells transfected with an N-terminal Flag-tagged human TLR9 expression vector (+) or an empty vector (−) and stained with an anti-Flag monoclonal antibody was examined by fluorescence-activated cell sorting.

HindIII-digested viral DNA and hCpG exhibited significant NF-κB activation, suggesting that undigested viral DNA is incapable of penetrating cells by transfection. No activation of NF-κB was observed in 293T cells cotransfected with a human TLR2 or TLR4 expression plasmid when stimulated with digested AcNPV DNA (data not shown).

Recent work demonstrated that the endogenous expression of TLR3, TLR7, TLR8, and TLR9 was mainly detected in the cytoplasmic vesicles of macrophages (58). To examine the localization of transiently expressed TLR9, we transfected 293T cells with a TLR9 expression plasmid and examined TLR9 expression by immunofluorescence microscopy and cell sorting. The expression of TLR9 in the cytoplasm was three times higher than that at the cell surface (Fig. 6B and C). These results indicate that the introduction of AcNPV DNA into the cytoplasm is specifically detected by human TLR9 and results in the activation of NF-κB.

AcNPV requires endosomal maturation to induce immune system activation in macrophages. To further explore the role of endocytosis in the signal transduction pathway triggered by AcNPV DNA, we examined the effect of endosomal maturation or acidification inhibitors. As shown in Fig. 7A, chloroquine was able to inhibit immune system activation of RAW264.7 cells treated with AcNPV and mCpG oligonucleotides in a dose-dependent manner, but no inhibition of LPS or PGN activation was observed. Other inhibitors of endoso-

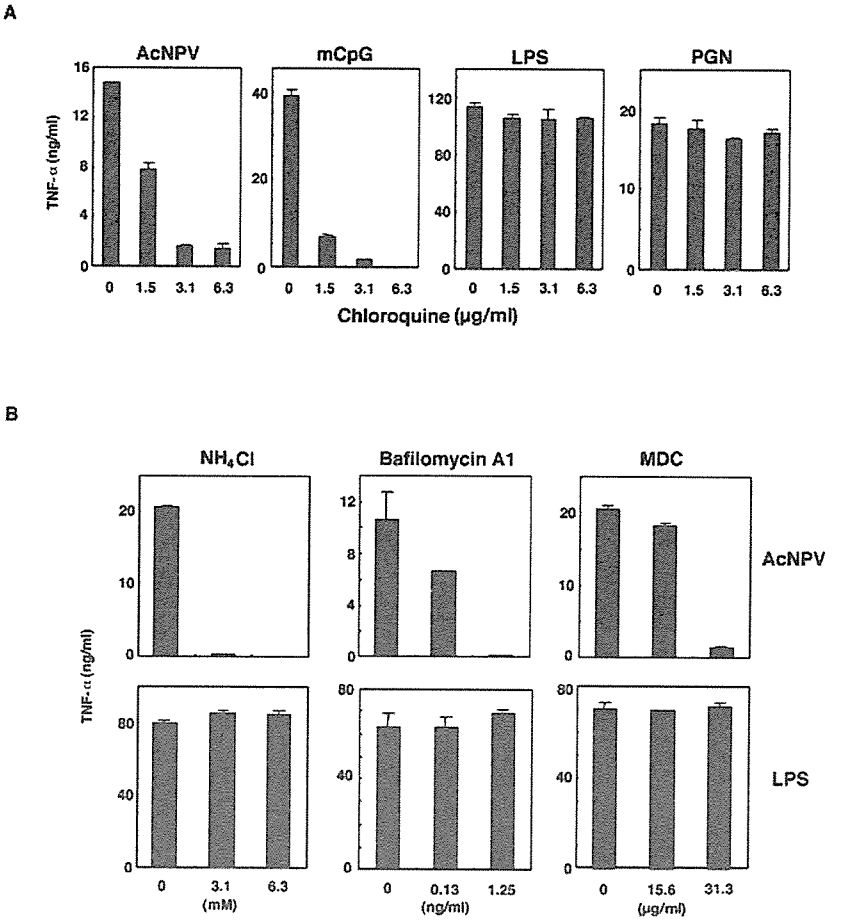

FIG. 7. AcNPV requires endosomal maturation to induce immune system activation in macrophages. (A) RAW264.7 cells (10^6 cells/well) were stimulated with AcNPV (5 μg/ml), mCpG (200 ng/ml), LPS (10 ng/ml), or PGN (2.5 μg/ml) at the indicated concentrations of chloroquine. After 24 h of incubation, the production of TNF-α in culture supernatants was determined by a sandwich ELISA. Chloroquine was added to the cells 2 h before stimulation. Data are shown as means ± SD. (B) RAW264.7 cells (10^6 cells/well) were treated with AcNPV (5 μg/ml) or LPS (10 ng/ml) and with the indicated concentrations of endosomal maturation inhibitors. After 24 h of incubation, the production of TNF-α in culture supernatants was determined by a sandwich ELISA. The inhibitors were added to the cells 2 h before stimulation. Data are shown as means ± SD.

mal maturation, such as ammonium chloride, bafilomycin A1, and MDC, inhibited AcNPV-induced, but not LPS-induced, immune system activation (Fig. 7B). Together with our other data, these results indicate that endosomal acidification and/or maturation is a key step in AcNPV-induced immune system activation via TLR9, a process that requires the release of the viral genome into TLR9-expressing cytoplasmic vesicles following the internalization of viral DNA by endocytosis through gp64-mediated membrane fusion.

AcNPV penetrates macrophages via the phagocytic pathway. To further confirm that baculovirus was internalized into macrophages, we inoculated RAW264.7 cells with a recombinant baculovirus carrying a luciferase gene under the control of a mammalian promoter, AcCAGluc (49). As shown in Fig. 8A, the expression of luciferase was observed in 293T cells, but not RAW264.7 cells, that were infected with AcCAGluc. The viral capsid protein was clearly detected by immunoblotting for both 293T and RAW264.7 cells infected with AcNPV, but the protein level was greatly diminished in RAW264.7 cells by 6 h postinoculation, probably as a result of degradation (Fig. 8B). These results suggest that baculovirus can penetrate into different cells via gp64-mediated endocytosis but that it translocates into different subcellular compartments in different cells. In 293T cells, the nucleocapsid was apparently able to reach the nucleus, where the reporter gene was efficiently transcribed following uncoating. However, in the immunocompetent RAW264.7 cells, the nucleocapsid appeared to have been trapped by the phagocytic pathway, and degraded viral DNA was then translocated into TLR9-expressing intracellular compartments (58).

DISCUSSION

We have previously demonstrated that intranasal inoculation with AcNPV induces a strong innate immune response that protects mice from a lethal challenge with influenza virus (1). The lungs of mice inoculated with AcNPV exhibited a marked infiltration of macrophages, which presumably inhibit the growth of influenza virus in the lung tissues. The baculovirus envelope glycoprotein gp64 contains mannose, fucose,

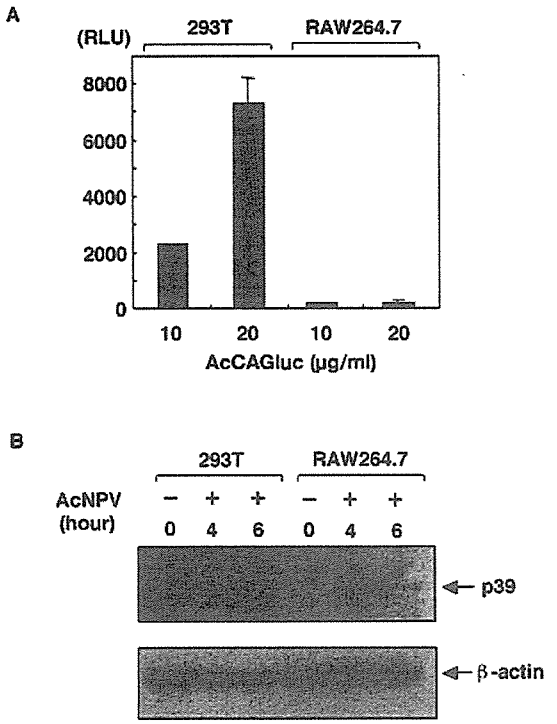

FIG. 8. AcNPV penetrates macrophages through the phagocytic pathway. (A) 293T and RAW264.7 cells (10^6 cells/well) were inoculated with a recombinant baculovirus possessing the luciferase gene under the control of the CAG promoter, AcCAGluc (49) (10 and 20 μg/ml). Cells were harvested 24 h after infection, and relative luciferase activities were determined. (B) 293T and RAW264.7 cells (10^6 cells/well) were inoculated with AcCAGluc (40 μg/ml), washed extensively after 1 h of adsorption, and harvested after 4 or 6 h of incubation. The presence of the p39 capsid protein in cells inoculated with AcNPV was determined by immunoblotting with an anti-p39 monoclonal antibody.

and *N*-acetyl-glucosamine modifications but no detectable galactose or terminal sialic acid residues (29). The mannose receptor (MR) recognizes a range of carbohydrates present on the surfaces and cell walls of microorganisms. MR is primarily expressed on macrophages and DCs and is involved in MR-mediated endocytosis and phagocytosis. In addition, MR plays a key role in host defense and the induction of innate immunity (8). Therefore, it is tempting to speculate that gp64 interacts with MR through its mannose modifications in macrophages and DCs of mice inoculated with AcNPV. However, our data contradict such a model; instead, we show that it is AcNPV DNA, not the gp64 glycoprotein, that induces immune system activation in a MyD88/TLR9-dependent manner.

Recently, it was shown that plasmacytoid DCs (pDCs) naturally produce IFN-α in response to viruses (30). HSV-1 and -2, whose genomes contain abundant CpG motifs, are able to induce the production of IFN-α in pDCs. The HSV-induced production of IFN-α in pDCs derived from MyD88- and TLR9-deficient mice was completely eliminated (33, 40). The recognition of the HSV genome by TLR9 was shown to be mediated by an endocytic pathway that can be inhibited by chloroquine or bafilomycin A1. In this study, we demonstrated that AcNPV induces proinflammatory cytokines through a MyD88/TLR9-dependent signaling pathway, whereas signaling molecules other than MyD88 may participate in IFN-α production in response to AcNPV. Recently, MyD88-independent TLR signaling events involving TIR domain-containing adaptor inducing IFN-β (TRIF) were described (59). Therefore, it is possible that the TRIF pathway is one means by which AcNPV induces MyD88-independent IFN production. However, future studies are needed to clarify the precise mechanisms of this induction.

While UV irradiation of AcNPV abolishes its ability to stimulate an immune response, the addition of liposomes is able to restore this activity. UV-inactivated HSV is capable of inducing the production of IFN-α in pDCs (40), indicating that viral replication is not required for the HSV-induced immune response. In contrast, UV irradiation of AcNPV abolishes immune stimulation in macrophages, while internalization of the inactivated virus by liposomes restores the activity. These results, in conjunction with our data for AcNPVΔ64, indicate that the AcNPV-induced production of cytokines in immunocompetent cells requires a fusion process mediated by gp64 that leads to internalization of the viral genome into the cells.

Recently, several viral envelope glycoproteins were shown to induce immune system activation through TLRs (10, 22, 34, 47). However, gp64 does not directly participate in a TLR-mediated immune response. TLR family members are expressed differentially at very low levels on the surfaces of different immune cells and appear to respond to different stimuli (43). A recent study indicated that LPS and CpG-rich DNA activate TLRs in distinct cellular compartments (3). Internalization and endosomal maturation are required for CpG-rich DNA to activate TLR9, but not for LPS to activate TLR4 on the plasma membrane. We showed here that the inhibition of endosomal maturation by a treatment with chloroquine abolishes the immune system activation of AcNPV in a dose-dependent manner. These results imply that immune system activation by AcNPV through TLR9 requires membrane fusion via gp64 as well as the liberation of the viral genome into cytoplasmic vesicles expressing TLR9.

Interestingly, Lund et al. demonstrated that the TLR7-mediated immune recognition of single-stranded RNAs from vesicular stomatitis virus and influenza virus requires endosomal acidification (41). The recognition of HSV-1 and HSV-2 viral DNAs through a TLR9/MyD88-dependent pathway in pDCs also requires endosomal acidification (40). These data indicate that TLR7 and TLR9 expressed in the endosomal or lysosomal compartments of immunocompetent cells recognize the viral genome entering the cell through receptor-mediated endocytosis or phagocytosis, leading to the secretion of inflammatory cytokines and IFNs. However, the precise mechanisms by which viral genomes translocate to TLR-expressing compartments are still unknown.

Since the first report on the immunostimulatory potential of bacterial DNA, which found that the main immunogenic fraction of mycobacterial lysates consists of genomic DNA (55, 56), substantial progress has been made towards understanding the immunostimulatory potency of CpG-rich DNA motifs, which are more common in bacteria than in vertebrates. For instance, TLR9 was shown to be responsible in vivo for immune system stimulation by oligodeoxynucleotides containing unmethylated CpG motifs (24). Like bacteria, AcNPV contains a significant

number of potentially bioactive CpG motifs. Interestingly, the frequency of CpG motifs in HSV DNA, which has been shown to be involved in the induction of angiogenesis in stromal keratitis (61), was similar to that in *E. coli* DNA. In contrast, the frequency of CpG motifs in the genome of an insect poxvirus was much lower than that for AcNPV (Table 1).

In conclusion, we have demonstrated that AcNPV has the ability to induce innate immune system activation through a MyD88/TLR9-dependent pathway. The molecular mechanisms of viral uptake, intracellular processing, and the induction of potent antiviral activity in immune cells require further investigation. However, the strong immune response induced by AcNPV makes it a promising candidate for a novel, adjuvant-containing vaccine vehicle against infectious diseases. In particular, our findings raise the possibility that AcNPV may be harnessed therapeutically to induce a host immune response against various infectious diseases caused by pathogens invading the respiratory tract.

ACKNOWLEDGMENTS

We are grateful to T. H. Chuang for providing us with the TLR9 expression plasmid, D. T. Golenbock for the pELAM Luc plasmid, and G. F. Rohrmann for the p39 monoclonal antibody. We also thank I. Yanase and H. Murase for secretarial work. T.A. and H.H. are Research Fellows of the Japan Society for the Promotion of Science.

This work was supported by grants-in-aid from the Ministry of Health, Labor and Welfare in Japan to Y.M. and from the 21st Century Center of Excellence Program of Japan to Y.M. and S.A.

REFERENCES

1. **Abe, T., H. Takahashi, H. Hamazaki, N. Miyano-Kurosaki, Y. Matsuura, and H. Takaku.** 2003. Baculovirus induces an innate immune response and confers protection from lethal influenza virus infection in mice. J. Immunol. **171**:1133–1139.
2. **Adachi, O., T. Kawai, K. Takeda, M. Matsumoto, H. Tsutsui, M. Sakagami, K. Nakanishi, and S. Akira.** 1998. Targeted disruption of the MyD88 gene results in loss of IL-1- and IL-18-mediated function. Immunity **9**:143–150.
3. **Ahmad-Nejad, P., H. Hacker, M. Rutz, S. Bauer, R. M. Vabulas, and H. Wagner.** 2002. Bacterial CpG-DNA and lipopolysaccharides activate Toll-like receptor at distinct cellular compartments. Eur. J. Immunol. **32**:1958–1968.
4. **Airenne, K. J., M. O. Hiltunen, M. P. Turunen, A. M. Turunen, O. H. Laitinen, M. S. Kulomaa, and S. Y. Herttuala.** 2000. Baculovirus-mediated periadventitial gene transfer to rabbit carotid artery. Gene Ther. **7**:1499–1504.
5. **Akira, S., K. Takeda, and T. Kaisho.** 2001. Toll-like receptors: critical proteins linking innate and acquired immunity. Nat. Immunol. **2**:675–680.
6. **Alexopoulou, L., A. C. Holt, R. Medzhitov, and R. A. Flavell.** 2001. Recognition of double-stranded RNA and activation of NF-κB by Toll-like receptor 3. Nature **413**:732–738.
7. **Aliprantis, A. O., R. B. Yang, M. R. Mark, S. Suggett, B. Devaux, J. D. Radolf, G. R. Klimpel, P. Godowski, and A. Zychlinsky.** 1999. Cell activation and apoptosis by bacterial lipoproteins through Toll-like receptor-2. Science **285**:736–739.
8. **Apostolopoulos, V., and I. F. McKenzie.** 2001. Role of the mannose receptor in the immune response. Curr. Mol. Med. **1**:469–474.
9. **Barsoum, J., R. Brown, M. Mckee, and F. M. Boyce.** 1997. Efficient transduction of mammalian cells by a recombinant baculovirus having the vesicular stomatitis virus G glycoprotein. Hum. Gene Ther. **8**:2011–2018.
10. **Bieback, K., E. Lien, I. M. Klagge, E. Avota, J. Schneider-Schaulies, W. P. Duprex, H. Wagner, C. J. Kirschning, V. Ter Meulen, and S. Schneider-Schaulies.** 2002. Hemagglutinin protein of wild-type measles virus activates Toll-like receptor 2 signaling. J. Virol. **76**:8729–8736.
11. **Bowie, A., E. Kiss-Toth, J. A. Symons, G. L. Smith, S. K Dower, and L. A. O. Neill.** 2000. A46R and A52R from vaccinia virus are antagonists of host IL-1 and Toll-like receptor signaling. Proc. Natl. Acad. Sci. USA **97**:10162–10167.
12. **Boyce, F. M., and N. L. R. Bucher.** 1996. Baculovirus mediated gene transfer into mammalian cells. Proc. Natl. Acad. Sci. USA **93**:2348–2352.
13. **Brightbill, H. D., D. H. Libraty, S. R. Krutzik, R. B. Yang, J. T. Belisle, J. R. Bleharski, M. Maitland, M. V. Norgard, S. E. Plevy, S. T. Smale, P. J. Brennan, B. R. Bloom, P. J. Godowski, and R. L. Modlin.** 1999. Host defense mechanisms triggered by microbial lipoproteins through Toll-like receptors. Science **285**:732–736.
14. **Chuang, T. H., J. Lee, L. Kline, J. C. Mathison, and R. J. Ulevitch.** 2002. Toll-like receptor 9 mediates CpG-DNA signaling. J. Leukoc. Biol. **71**:538–544.
15. **Compton, T., E. A. Kurt-Jones, K. W. Boehme, J. Belko, E. Latz, D. T. Golenbock, and R. W. Finberg.** 2003. Human cytomegalovirus activates inflammatory cytokine responses via CD14 and Toll-like receptor 2. J. Virol. **77**:4588–4596.
16. **Condreay, J. P., S. M. Witherspoon, W. C. Clay, and T. A. Kost.** 1999. Transient and stable gene expression in mammalian cells transduced with a recombinant baculovirus vector. Proc. Natl. Acad. Sci. USA **96**:127–132.
17. **Diebold, S. S., T. Kaisho, H. Hemmi, S. Akira, E. Reis, and C. Sousa.** 2004. Innate antiviral responses by means of TLR7-mediated recognition of single-stranded RNA. Science **303**:1529–1531.
18. **Gronowski, A. M., D. M. Hilbert, K. C. F. Sheehan, G. Garotta, and R. D. Schreiber.** 1999. Baculovirus stimulates antiviral effect in mammalian cells. J. Virol. **73**:9944–9951.
19. **Hacker, H., H. Mischak, T. Miethke, S. Liptay, R. Schmid, T. Sparwasser, K. Heeg, G. B. Lipford, and H. Wagner.** 1998. CpG-DNA-specific activation of antigen-presenting cells requires stress kinase activity and is preceded by non-specific endocytosis and endosomal maturation. EMBO J. **17**:6230–6240.
20. **Hacker, H., R. M. Vabulas, O. Takeuchi, K. Hoshino, S. Akira, and H. Wagner.** 2000. Immune cell activation by bacterial CpG-DNA through myeloid differential marker 88 and tumor necrosis factor receptor-associated factor (TRAF) 6. J. Exp. Med. **192**:595–600.
21. **Hayashi, F., K. D. Smith, A. Ozinsky, T. R. Hawn, E. C. Yi, D. R. Goodlett, J. K. Eng, S. Akira, D. M. Underhill, and A. Aderem.** 2001. The innate immune response to bacterial flagellin is mediated by Toll-like receptor 5. Nature **410**:1099–1103.
22. **Haynes, L. M., D. D. Moore, E. A. Kurt-Jones, R. W. Finberg, L. J. Anderson, and R. A. Tripp.** 2001. Involvement of Toll-like receptor 4 in innate immunity to respiratory syncytial virus. J. Virol. **75**:10730–10737.
23. **Heil, F., H. Hemmi, H. Hochrein, F. Ampenberger, C. Kirschning, S. Akira, G. Lipford, H. Wagner, and S. Bauer.** 2004. Species-specific recognition of single-stranded RNA via Toll-like receptor 7 and 8. Science **303**:1526–1529.
24. **Hemmi, H., O. Takeuchi, T. Kawai, T. Kaisho, S. Sato, H. Sanjo, M. Matsumoto, K. Hoshino, H. Wagner, K. Takeda, and S. Akira.** 2000. A Toll-like receptor recognizes bacterial DNA. Nature **408**:740–745.
25. **Hemmi, H., T. Kaisho, O. Takeuchi, S. Sato, H. Sanjo, K. Hoshino, T. Horiuchi, H. Tomizawa, K. Takeda, and S. Akira.** 2002. Small anti-viral compounds activate immune cells via the TLR7 MyD88-dependent signaling pathway. Nat. Immunol. **3**:196–200.
26. **Hofmann, C., V. Sandig, G. Jennings, M. Rudolph, P. Schlag, and M. Strauss.** 1995. Efficient gene transfer into human hepatocytes by baculovirus vectors. Proc. Natl. Acad. Sci. USA **92**:10099–10103.
27. **Hoshino, K., O. Takeuchi, T. Kawai, H. Sanjo, T. Ogawa, Y. Takeda, K. Takeda, and S. Akira.** 1999. Cutting edge: Toll-like receptor 4 (TLR4)-deficient mice are hyporesponsive to lipopolysaccharide: evidence for TLR4 as the LPS gene product. J. Immunol. **162**:3749–3752.
28. **Huser, A., M. Rudolph, and C. Hofmann.** 2001. Incorporation of decay-accelerating factor into the baculovirus envelope generates complement resistant gene transfer vectors. Nat. Biotechnol. **19**:451–455.
29. **Jarvis, D. L., and E. E. Finn.** 1995. Biochemical analysis of the N-glycosylation pathway in baculovirus-infected lepidopteran insect cells. Virology **212**:500–511.
30. **Kadowaki, N., S. Antonenko, J. Y. Lau, and Y. J. Liu.** 2000. Natural interferon alpha/beta-producing cells link innate and adaptive immunity. J. Exp. Med. **192**:219–226.
31. **Kawai, T., O. Takeuchi, T. Fujita, J. Inoue, P. F. Muhlradt, S. Sato, K. Hoshino, and S. Akira.** 2001. Lipopolysaccharide stimulates the MyD88-independent pathway and results in activation of IFN-regulatory factor 3 and the expression of a subset of lipopolysaccharide-inducible genes. J. Immunol. **167**:5887–5894.
32. **Krieg, A. M., and H. Wagner.** 2000. Causing a commotion in the blood: immunotherapy progresses from bacteria to bacterial DNA. Immunol. Today **21**:521–526.
33. **Krug, A., G. D. Luker, W. Barchet, D. A. Leib, S. Akira, and M. Colonna.** 2004. Herpes simplex virus type 1 (HSV-1) activates murine natural interferon-producing cells (IPC) through Toll-like receptor 9. Blood **103**:1433–1437.
34. **Kurt-Jones, E. A., L. Popova, L. Kwinn, L. M. Haynes, L. P. Jones, R. A. Tripp, E. E. Walsh, M. W. Freeman, D. T. Golenbock, L. J. Anderson, and R. W. Finberg.** 2000. Pattern recognition receptors TLR4 and CD14 mediate response to respiratory syncytial virus. Nat. Immunol. **5**:398–401.
35. **Kurt-Jones, E. A., M. Chan, S. Zhou, J. Wang, G. Reed, R. Bronson, M. M. Arnold, D. M. Knipe, and R. W. Finberg.** 2004. Herpes simplex virus 1 interaction with Toll-like receptor 2 contributes to lethal encephalitis. Proc. Natl. Acad. Sci. USA **101**:1315–1320.
36. **Lee, J., T. H. Chuang, V. Redecke, L. She, P. M. Pitha, D. A. Carson, E. Raz, and H. B. Cottam.** 2003. Molecular basis for the immunostimulatory activity of guanine nucleoside analogs: activation of Toll-like receptor 7. Proc. Natl. Acad. Sci. USA **100**:6646–6651.

37. **Lehtolainen, P., K. Tyynela, J. Kannasto, K. J. Airenne, and S. Y. Herttuala.** 2002. Baculoviruses exhibit restricted cell type specificity in rat brain: a comparison of baculovirus- and adenovirus-mediated intracerebral gene transfer in vivo. Gene Ther. **9:**1693–1699.
38. **Lematitre, B., E. Nicolas, L. Michaut, J. M. Reichhart, and J. A. Hoffmann.** 1996. The dorsoventral regulatory gene cassette spatzle/Toll/cactus controls the potent antifungal response in Drosophila adults. Cell **86:**973–983.
39. **Luckow, V. A., and M. D. Summers.** 1988. Signals important for high-level expression of foreign genes in Autographa californica nuclear polyhedrosis virus expression vectors. Bio/Technology **6:**47–55.
40. **Lund, J., A. Sato, S. Akira, R. Medzhitov, and A. Iwasaki.** 2003. Toll-like receptor 9-mediated recognition of herpes simplex virus-2 by plasmacytoid dendritic cells. J. Exp. Med. **198:**513–520.
41. **Lund, J., L. Alexopoulou, A. Sato, M. Karow, N. C. Adams, N. W. Gale, A. Iwasaki, and R. A. Flavell.** 2004. Recognition of single-stranded RNA viruses by Toll-like receptor 7. Proc. Natl. Acad. Sci. USA **101:**5598–5603.
42. **Matsuura, Y., R. D. Possee, H. A. Overton, and D. H. L. Bishop.** 1987. Baculovirus expression vector. The requirement for high level expression of proteins, including glycoproteins. J. Gen. Virol. **68:**1233–1250.
43. **Muzio, M., D. Bosisio, N. Polentarutti, G. Damico, A. Stoppacciaro, R. Mancinelli, C. vant Veer, G. Penton-Rol, L. P. Ruco, P. Allavena, and A. Mantovani.** 2000. Differential expression and regulation of Toll-like receptors (TLR) in human leukocytes: selective expression of TLR3 in dendritic cells. J. Immunol. **164:**5998–6004.
44. **Ozinsky, A., D. M. Underhill, J. D. Fontenot, A. M. Hajjar, K. D. Smith, C. B. Wilson, L. Schroeder, and A. Aderem.** 2000. The repertoire for pattern recognition of pathogens by the innate immune system is defined by cooperation between Toll-like receptors. Proc. Natl. Acad. Sci. USA **97:**13766–13771.
45. **Pieroni, L., D. Maione, and N. L. Monica.** 2001. In vivo gene transfer in mouse skeletal muscle mediated by baculovirus vectors. Hum. Gene Ther. **12:**871–881.
46. **Poltorak, A., X. He, I. Smirnova, M. Y. Liu, C. Van Huffel, X. Du, D. Birdwell, E. Alejos, M. Silva, C. Galanos, M. Freudenberg, P. Ricciardi-Castagnoli, B. Layton, and B. Beutler.** 1998. Defective LPS signaling in C3H/HeJ and C57BL/10ScCr mice: mutations in Tlr4 gene. Science **282:**2085–2088.
47. **Rassa, J. C., J. L. Meyers, Y. Zhang, R. Kudaravalli, and S. R. Ross.** 2002. Murine retroviruses activate B cells via interaction with Toll-like receptor 4. Proc. Natl. Acad. Sci. USA **99:**2281–2286.
48. **Sandig, V., C. Hofmann, S. Steinert, G. Jennings, P. Schlag, and M. Strauss.** 1996. Gene transfer into hepatocytes and human liver tissue by baculovirus vectors. Hum. Gene Ther. **7:**1937–1945.
49. **Shoji, I., H. Aizaki, H. Tani, K. Ishii, T. Chiba, I. Saito, T. Miyamura, and Y. Matsuura.** 1997. Efficient gene transfer into various mammalian cells, including non-hepatic cells, by baculovirus vectors. J. Gen. Virol. **78:**2657–2664.
50. **Takeuchi, O., K. Hoshino, T. Kawai, H. Sanjo, H. Takeda, T. Ogawa, K. Takeda, and S. Akira.** 1999. Differential roles of TLR2 and TLR4 in recognition of gram-negative and gram-positive bacterial cell wall components. Immunity **11:**443–451.
51. **Takeuchi, O., and S. Akira.** 2001. Toll-like receptors: their physiological role and signal transduction system. Int. Immunopharmacol. **1:**625–635.
52. **Takeuchi, O., A. Kaufmann, K. Grote, T. Kawai, K. Hoshino, M. Morr, P. F. Muhlradt, and S. Akira.** 2000. Cutting edge: preferentially the R-stereoisomer of the mycoplasmal lipopeptide macrophage-activating lipopeptide-2 activates immune cells through a Toll-like receptor 2- and MyD88-dependent signaling pathway. J. Immunol. **164:**554–557.
53. **Tani, H., M. Nishijima, H. Ushijima, T. Miyamura, and Y. Matsuura.** 2001. Characterization of cell-surface determinants important for baculovirus infection. Virology **279:**343–353.
54. **Tani, H., C. K. Limn, C. C. Yap, M. Onishi, M. Nozaki, Y. Nishimune, N. Okahashi, Y. Kitagawa, R. Watanabe, R. Mochizuki, K. Moriishi, and Y. Matsuura.** 2003. In vitro and in vivo gene delivery by recombinant baculoviruses. J. Virol. **77:**9799–9808.
55. **Tokunaga, T., H. Yamamoto, S. Shimada, H. Abe, T. Fukuda, Y. Fujisawa, Y. Furutani, O. Yano, T. Kataoka, T. Sudo, N. Makiguchi, and T. Suganuma.** 1984. Antitumor activity of deoxyribonucleic acid fraction from Mycobacterium bovis BCG. I. Isolation, physicochemical characterization and antitumor activity. JNCI **72:**955–962.
56. **Tokunaga, T., T. Yamamoto, and S. Yamamoto.** 1999. How BCG led to the discovery of immunostimulatory DNA. Jpn. J. Infect. Dis. **52:**1–11.
57. **Underhill, D. M., A. Ozinsky, A. M. Hajjar, A. Stevens, C. B. Wilson, M. Bassetti, and A. Aderem.** 1999. The Toll-like receptor 2 is recruited to macrophage phagosomes and discriminates between pathogens. Nature **401:**811–815.
58. **Wagner, H.** 2004. The immunobiology of the TLR9 subfamily. Trends Immunol. **25:**381–386.
59. **Yamamoto, M., S. Sato, H. Hemmi, K. Hoshino, T. Kaisho, H. Sanjo, O. Takeuchi, M. Sugiyama, M. Okabe, K. Takeda, and S. Akira.** 2003. Role of adaptor TRIF in the MyD88-independent Toll-like receptor signaling pathway. Science **301:**640–643.
60. **Zhang, D., G. Zhang, M. S. Hayden, M. B. Greenblatt, C. Bussey, R. A. Flavell, and S. Ghosh.** 2004. A Toll-like receptor that prevents infection by uropathogenic bacteria. Science **303:**1522–1526.
61. **Zheng, M., D. M. Klinman, M. Gierynska, and B. T. Rouse.** 2002. DNA containing CpG motifs induces angiogenesis. Proc. Natl. Acad. Sci. USA **99:**8944–8949.

Available online at www.sciencedirect.com
SCIENCE DIRECT®
Biochemical and Biophysical Research Communications 319 (2004) 1228–1234
BBRC
www.elsevier.com/locate/ybbrc

Phosphorylation of p38 MAPK and its downstream targets in SARS coronavirus-infected cells

Tetsuya Mizutani,* Shuetsu Fukushi, Masayuki Saijo, Ichiro Kurane, and Shigeru Morikawa

Special Pathogens Laboratory, Department of Virology 1, National Institute of Infectious Diseases, Gakuen 4-7-1, Musashimurayama, Tokyo 208-0011, Japan

Received 3 March 2004
Available online 7 June 2004

Abstract

Severe acute respiratory syndrome (SARS) has become a global public health emergency. Understanding the molecular mechanisms of SARS-induced cytopathic effects (CPEs) is a rational approach for the prevention of SARS, and an understanding of the cellular stress responses induced by viral infection is important for understanding the CPEs. Polyclonal antibodies, which recognized nucleocapsid (N) and membrane (M) proteins, detected viral N and M proteins in virus-infected Vero E6 cells at least 6 and 12 h post-infection (h.p.i.), respectively. Furthermore, detection of DNA ladder and cleaved caspase-3 in the virus-infected cells at 24 h.p.i. indicated that SARS-CoV infection induced apoptotic cell death. Phosphorylation of p38 MAPK was significantly up-regulated at 18 h.p.i. in SARS-CoV-infected cells. The downstream targets of p38 MAPK, MAPKAPK-2, HSP-27, CREB, and eIF4E were phosphorylated in virus-infected cells. The p38 MAPK inhibitor, SB203580, inhibited effectively phosphorylation of HSP-27, CREB, and eIF4E in SARS-CoV-infected cells. However, viral protein synthesis was not affected by treatment of SB203580.

Severe acute respiratory syndrome coronavirus (SARS-CoV) is the etiological agent responsible for the outbreak of SARS, an extremely severe disease that has spread to many countries throughout the world. In the period from February to June 2003, 32 countries were affected by SARS. SARS-CoV is a positive-strand RNA virus, and its genome is composed of about 29,700 nucleotides. The genomic organization of SARS-CoV is that of a typical coronavirus, and sequentially contains genes encoding polymerase (and polymerase-related proteins), spike, envelope, membrane (M), and nucleocapsid (N) proteins. Three groups of coronaviruses were known prior to SARS, while phylogenic analysis indicated SARS-CoV to be a member of a fourth group [1,2]. A vaccine is currently under development and there is no efficacious therapy for SARS.

Mitogen-activated protein kinases (MAPKs) are signal transducers that respond to extracellular stimulation by cytokines, growth factors, viral infection, and stress, and in turn regulate cell differentiation, proliferation, survival, and apoptosis [3–6]. In particular, p38 MAPK is strongly activated by stress and inflammatory cytokines. In the case of mouse hepatitis virus (MHV), a prototype coronavirus, virus-infected cells showed induction of p38 MAPK [7]. The SARS-CoV N protein has been reported to be involved in the regulation of cellular signaling pathways [8]. The levels of transcription factors binding to promoter sequences of c-Fos, ATF-2, CREB-1, and Fos B, which are related to AP-1, were increased by expression of N protein. However, there have been no previous reports regarding activation of signaling pathways by infection with SARS-CoV. In addition, no information is available regarding the molecular mechanisms of the cytopathic effects of SARS-CoV-infection. In the present study, we demonstrated that infection of Vero E6 cells by SARS-CoV induced apoptotic cell death and that p38 MAPK and its downstream targets were phosphorylated during viral replication. Understanding the mechanisms of p38

* Corresponding author. Fax: +81-42-565-3315.
E-mail address: tmizutan@nih.go.jp (T. Mizutani).

0006-291X/$ - see front matter © 2004 Elsevier Inc. All rights reserved.
doi:10.1016/j.bbrc.2004.05.107

MAPK activation may lead to successful strategies for targeting these molecules in the therapy of SARS.

Materials and methods

Cells and virus. Vero E6 cells were routinely subcultured in 75-cm^3 flasks in Dulbecco's modified Eagle's medium (DMEM, Sigma, St. Louis, MO, USA) supplemented with 0.2 mM L-glutamine, 100 U/ml penicillin, 100 μg/ml streptomycin, and 5% (v/v) fetal bovine serum (FBS), and maintained at 37 °C in an atmosphere of 5% CO_2. For use in the experiments, the cells were split once they reached 90% confluence and seeded onto 6-well or 24-well tissue culture plate inserts. The culture medium was changed to 2% FBS containing DMEM prior to virus infection. In this study, we used SARS-CoV [9], which was isolated as Frankfurt 1 [10] and kindly provided by Dr. J. Ziebuhr. The seed virus was passaged at least seven times, including one passage in our laboratory. Infection was usually performed with a multiplicity of infection (m.o.i.) of 5. The cells were stained with 0.05% crystal violet after fixing with 10% formaldehyde.

Anti-SARS-CoV antibodies. Two peptides, RYRIGNYKLNTD (GenBank Accession No. AAP13571; residues 197–208) and RRVRGGDGKMKE (GenBank Accession No. AAP13814; residues 93–194), corresponding to fragments of the amino acid sequences of membrane (M) and nucleocapsid (N) proteins of SARS-CoV, respectively, were synthesized (Sigma Genosys, Ishikari, Japan). Rabbits were injected with the mixture of peptides (New Drug Development Research Center, Iwamizawa, Japan), and the polyclonal rabbit antisera were used for Western blotting analysis.

Western blotting. After viral infection at an m.o.i. of 5, whole-cell extracts were electrophoresed in 10% and 10–20% gradient polyacrylamide gels, and transferred onto PVDF membrane sheets (Immobilon-P, Millipore, Bedford, MA, USA). In this study, we applied two sets of samples to polyacrylamide gels, and the membranes were divided into two sheets after blotting. The following antibodies, obtained from Cell Signaling Technology (Beverly, MA, USA), were used in this study at a dilution of 1:1000: rabbit anti-phospho p38 MAPK (Thr180/Tyr182), rabbit anti-p38, rabbit anti-phospho MAPKAPK-2 (Thr334), anti-MAPKAPK-2, rabbit anti-phospho HSP-27 (Ser82), mouse anti-HSP-27, mouse anti-phospho CREB (Ser133), rabbit anti-CREB, anti-phospho eIF4E (Ser209), and anti-rabbit eIF4E. Rabbit anti-actin (H-196) (diluted 1:200) was obtained from Santa Cruz Biotechnology (Santa Cruz, CA, USA). After 15-h incubation, the membranes were washed with 0.1% TBS–Tween and specific proteins were detected with a ProtoBlot II AP system (Promega, Madison, WI, USA), as described previously [11].

DNA fragmentation. A MEBCYTO Apoptosis ladder detection kit (Medical and Biological Laboratories, Nagoya, Japan) was used for detection of DNA fragmentation. After viral infection, cells were lysed with lysis buffer. The cellular DNA was precipitated with ethanol, dried, and resuspended in Tris–EDTA buffer (10 mM Tris, 1 mM EDTA, pH 7.5) containing 100 μg/ml RNase A. The DNA solutions were incubated for 60 min at 37 °C. The DNA was analyzed by electrophoresis on 1% agarose gels and then stained with ethidium bromide.

Results and discussion

Detection of SARS-CoV-specific proteins in virus-infected cells

Vero E6 cells were infected with SARS-CoV at an m.o.i. of 5, and Western blotting analysis was performed using polyclonal rabbit serum (see Materials and methods) and cellular extracts obtained at 6, 12, 18, and 24 h.p.i. Nucleocapsid (N) and membrane (M) proteins of SARS-CoV were detected after 6 and 12 h.p.i., respectively (Fig. 1). Multiple bands appeared on the Western blots, because the M proteins of coronavirus are glycosylated and the N proteins are phosphorylated in the virally infected cells. These bands were not observed in extracts from cells that were not infected by SARS-CoV, indicating that the polyclonal rabbit sera specifically detected SARS-CoV proteins.

SARS-CoV induces apoptosis in virus-infected cells

The cytopathic effect (CPE) caused by SARS-CoV is focal with cell rounding [12], and we were clearly able to observe such CPEs at 24 h.p.i. (Fig. 2A), while mouse hepatitis virus (MHV), a prototype of coronavirus, causes cell-fusion after infection, and MHV infection induces apoptotic cell death in murine 17Cl-1 cells [13]. To confirm whether SARS-CoV-infection induces apoptosis in Vero E6 cells, cellular DNA was extracted from SARS-CoV-infected cells. At 24 h.p.i., DNA fragmentation typical of apoptosis was observed (Fig. 2B). Avian coronavirus infectious bronchitis virus (IBV) also induces apoptosis in infected Vero cells.

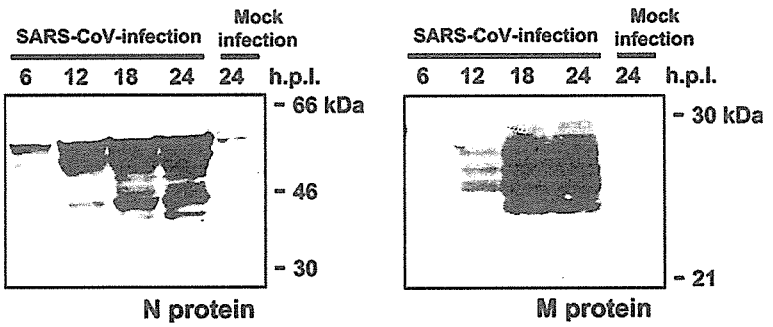

Fig. 1. Detection of SARS-CoV-specific proteins and activation of caspase-3 in virus-infected cells. Vero E6 cells were infected with SARS-CoV at an m.o.i. of 5, and Western blotting was then performed using proteins obtained at 6, 12, 18, and 24 h.p.i. Polyclonal antibodies against synthetic peptides based on membrane (M) and nucleocapsid (N) proteins were used.

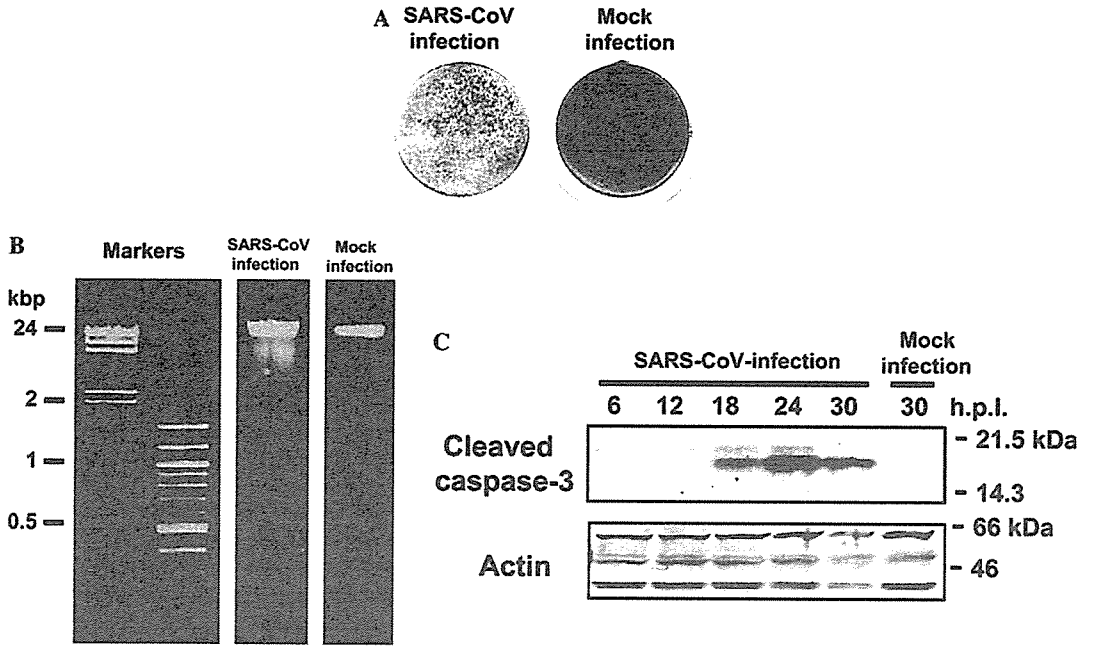

Fig. 2. Induction of apoptosis by SARS-CoV-infection. (A) Vero E6 cells were infected with SARS-CoV at an m.o.i. of 5 and stained with 0.05% crystal violet at 24 h.p.i. (B) DNA ladder fragmentation was detected at 24 h.p.i. (C) Western blotting analysis was performed using anti-cleaved caspase-3 antibody from 6, 12, 24, and 30 h.p.i. (C).

Caspase-3, which is one of the main effector caspases and is activated in response to both intracellular and extracellular death signals, was activated by IBV infection [14]. To confirm whether caspase-3 is activated by SARS-CoV-infection, Western blotting analysis was performed using anti-cleaved caspase-3 antibody. During apoptosis, caspase precursors are cleaved at Asp-X sites generating a large and a small subunit, which together constitute the active protease; the anti-caspase-3 antibody used in this study can specifically recognize the large fragment of cleaved caspase-3. As shown in Fig. 2C, the cleaved caspase-3 was detected in SARS-CoV-infected Vero E6 cells as a peak at 24 h.p.i. These results indicated that SARS-CoV induces apoptosis in the infected cells.

Activation of p38 MAPK in SARS-CoV-infected cells

Figs. 1 and 2 indicated that viral-specific proteins were synthesized at least 6 h.p.i., and the signaling pathway in response to stress should be activated from at least 6 to 24 h.p.i. by SARS-CoV-infection. Synthetic dsRNA poly(I)–poly(C) activates p38 MAPK and JNK/SAPK pathways in fibroblasts [15]: hence, double-stranded RNA intermediates of SARS-CoV that accumulate in infected cells may also trigger the p38 MAPK activation pathway. It was reported that p38 MAPK was activated in MHV-infected cells, and MHV replication has been shown to be necessary for p38 MAPK activation [7]. Therefore, the kinetics of p38 MAPK activation in SARS-CoV-infected Vero E6 cells were

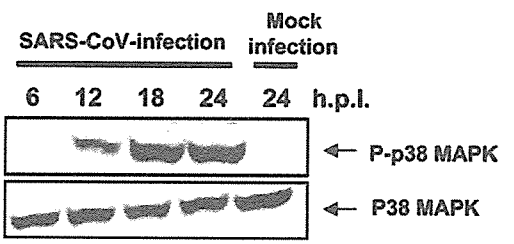

Fig. 3. Phosphorylation of p38 MAPK in SARS-CoV-infected Vero E6 cells. Phosphorylated and unphosphorylated p38 MAPK were detected by Western blotting analysis using proteins isolated from SARS-CoV-infected Vero E6 cells at 6, 12, 18, and 24 h.p.i.

analyzed. Vero E6 cells were infected with SARS-CoV at an m.o.i. of 5, and cell extracts were prepared at various times p.i. Western blotting analysis indicated an increase in the amount of phosphorylated p38 MAPK in the cells (Fig. 3). The p38 MAPK phosphorylation was not transient and reached the maximal level at 18 h.p.i. The role of p38 MAPK signaling pathway in cellular responses is diverse, depending on the cell type and stimulation. Thus, the p38 MAPK signaling pathway promotes both cell death and survival [16–18]. Therefore, investigation of the p38 MAPK-downstream targets is important to understand the mechanisms of cell death induced by SARS-CoV-infection.

MAPKAPK-2 and HSP-27 phosphorylation by SARS-CoV-infection

One of the downstream effectors of p38 MAPK is MAPK-activated protein kinase (MAPKAPK)-2, which

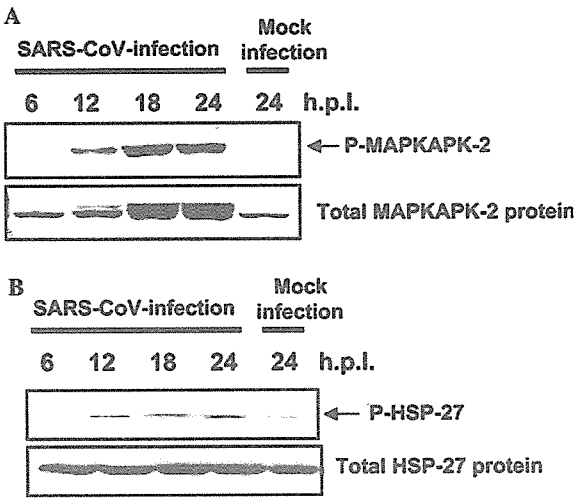

Fig. 4. Phosphorylation of MAPKAPK-2 and HSP-27 in virus-infected cells. (A) Phosphorylated and unphosphorylated MAPKAPK-2 were detected by Western blotting analysis. (B) Phosphorylated and unphosphorylated HSP-27 were detected by Western blotting analysis.

is activated in response to stress and growth factors [19,20]. We examined whether SARS-CoV-infection results in activation of this MAPKAPK-2 in Vero E6 cells. As shown in Fig. 4A, MAPKAPK-2 was phosphorylated in SARS-CoV-infected Vero E6 cells. To determine whether the substrates of MAPKAPK-2 are phosphorylated in the virus-infected cells, Western blotting analysis was performed using anti-phospho heat shock protein (HSP)-27. As shown in Fig. 4B, Hsp-27 was phosphorylated in SARS-CoV-infected cells at 12 h.p.i. A previous study showed that Hsp-27 has anti-apoptotic activity by inhibiting apoptosome formation [21].

Phosphorylation of transcription factors CREB and ATF-1

We next examined whether cAMP response element-binding protein (CREB), which is a substrate of mitogen- and stress-activated protein kinase (MSK)-1, was phosphorylated in infected cells. MSK-1 is thought to be a substrate of p38 MAPK and/or extracellular signal-related kinase (ERK)1/2. CREB was identified as an activator that responds to the cAMP-dependent signaling pathway and is also known to mediate an important survival signal under various conditions [22–24]. For example, the anti-apoptotic genes Bcl-2 and Bcl-xL are activated transcriptionally by phosphorylation of CREB in response to insulin-like growth factor (IGF)-I stimulation in PC-12 cells [25,26]. Immunoblot analysis (Fig. 5) indicated that the level of phosphorylated CREB was increased by SARS-CoV-infection. The anti-phospho CREB antibody used in this study also recognizes activation transcription factor (ATF)-1, which is a transcription factor. ATF-1 is a member of the CREB/ATF family that is phosphorylated by the cAMP-dependent protein kinase A (PKA) [27]. ATF-1 and CREB

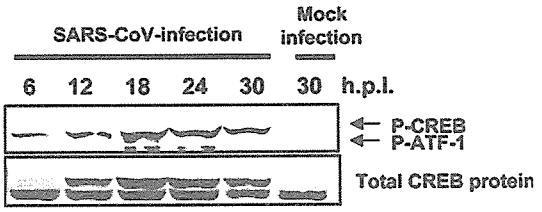

Fig. 5. Phosphorylation of CREB and ATF-1 in virus-infected cells. Phosphorylated and unphosphorylated CREB were detected by Western blotting analysis. Phosphorylated ATF-1 was also detected using anti-phospho CREB antibody.

act as survival factors [28]. This result suggested that phosphorylation of CREB and ATF-1 induces an anti-apoptotic environment in SARS-CoV-infected cells.

Phosphorylation of the translation initiation factor eIF4E

The translation initiation factor, eukaryotic initiation factor 4E (eIF4E), is phosphorylated by p38 MAPK and ERK1/2 [29,30], and eIF4E enhances translation rates of cap-containing mRNAs [31]. In the case of mouse hepatitis virus (MHV), eIF4E phosphorylation is utilized to promote virus-specific protein synthesis. Western blotting analysis was performed using anti-phospho eIF4E antibody. As shown in Fig. 6, the level of phosphorylated eIF4E was increased by SARS-CoV-infection.

Specific effective doses of p38 MAPK inhibitor

To confirm that the phosphorylation of downstream targets of p38 MAPK was specifically mediated by p38 MAPK, SB203580 (p38 MAPK-specific inhibitor), PD98059 (ERK1/2-specific inhibitor), and SP600125 (JNK-specific inhibitor) were used for inhibition of those function. Fifty percent confluency of Vero E6 cells were treated with 0, 10, 20, 30, 40, and 50 μM inhibitors in DMSO for 24, 48, and 72 h, and then cell viability was assayed using WST-1 system (Roche Diagnostics). Treating cells with up to 50 μM all inhibitors had little effect on cell viability (data not shown). Next, we examined the determination of specific inhibitory doses of

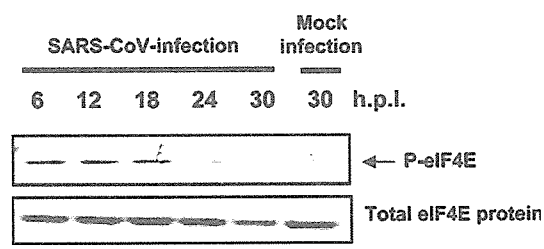

Fig. 6. Phosphorylation of eIF4E in virus-infected cells. Phosphorylated and unphosphorylated eIF4E were detected by Western blotting analysis.

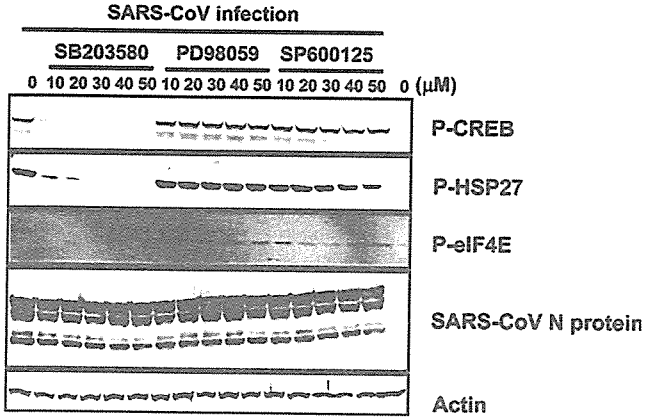

Fig. 7. Effective doses of p38 MAPK inhibitor. SARS-CoV-infected Vero E6 cells were treated with SB203580 (p38 MAPK-specific inhibitor), PD98059 (ERK1/2-specific inhibitor), and SP600125 (JNK-specific inhibitor) for 18 h. Western blot analysis was performed using anti-phosphorylated HSP-27, CREB eIF4E antibodies. SARS-CoV N protein was also detected.

p38 MAPK inhibitor in SARS-CoV-infected Vero E6 cells. SARS-CoV were infected to Vero E6 cells for 1 h, and then, three kinds of inhibitors were added to the cells. Proteins were harvested at 18 h.p.i. Western blot analysis was performed using anti-phospho CREB, HSP-27, and eIF4E antibodies (Fig. 7). The result shows that the eIF4E was effectively inhibited to be of phosphorylated type by p38 inhibitor between 10 and 50 μM. The effective dose for inhibition of CREB phosphorylation was more than 20 μM, and phosphorylated HSP-27 was not detected at 40 and 50 μM. Thus, this result indicated that CREB, HSP-27, and eIF4E were specifically phosphorylated by p38 MAPK, because both the ERK1/2 and JNK inhibitors did not inhibit those of phosphorylation between 10 and 50 μM. The 20 μM SB203580 was used in the study of MHV [7] and this concentration is known to efficiently block p38 MAPK activity in vivo [32]. Therefore, we used 20 and 30 μM SB 203580 in subsequent experiments.

No requirement for p38 MAPK phosphorylation of SARS-CoV replication

The p38 MAPK-dependent increase in eIF4E phosphorylation to promote virus-specific protein synthesis and subsequent progeny virus production were found in MHV [7]. Activated p38 MAPK and the downstream target, eIF4E, increased translation of MHV-specific proteins. We also found that eIF4E was activated in SARS-CoV-infection at 18 h.p.i. (Fig. 7). At that time of p.i., there was no significant difference in the amount of N protein of SARS-CoV among three inhibitor-treated cells and untreated cells. Kinetic study of N protein synthesis (Fig. 1A) showed that N protein seems to be the maximum amount in viral infected cells between 12 and 18 h.p.i. To investigate whether enhancement of virus-specific protein synthesis through virus-induced eIF4E activation occurs in SARS-CoV-infected cells, we tested the effect of p38 MAPK inhibitor, SB203580, on SARS-CoV-specific protein synthesis at early time p.i. Ten m.o.i. of SARS-CoV was inoculated in Vero E6 cells for 1 h, and then, the cells were washed two times. These cells were treated with 20 and 30 μM SB203580 for 6, 9, and 12 h.p.i. Western blot analysis showed that kinetics of SARS-CoV-specific protein accumulation in infected Vero E6 cells in the presence and absence of SB 203580 were similar (Fig. 8A). The phosphorylated eIF4E was detected at least 6 h.p.i. (Fig. 7) in SARS-CoV-infected cells. Taken together, SARS-CoV does not utilize activated eIF4E for its viral protein synthesis in Vero E6 cells. In addition, the CPEs caused by SARS-CoV-infection were slightly inhibited by SB203580 at late time p.i. (Fig. 8B).

In this study, we determined the cellular mechanisms by which SARS-CoV causes the activation of physiological intracellular signaling cascades that lead to the phosphorylation and activation of downstream molecules. We showed that SARS-CoV-infection of permissive cells induced the p38 MAPK signaling pathway. As

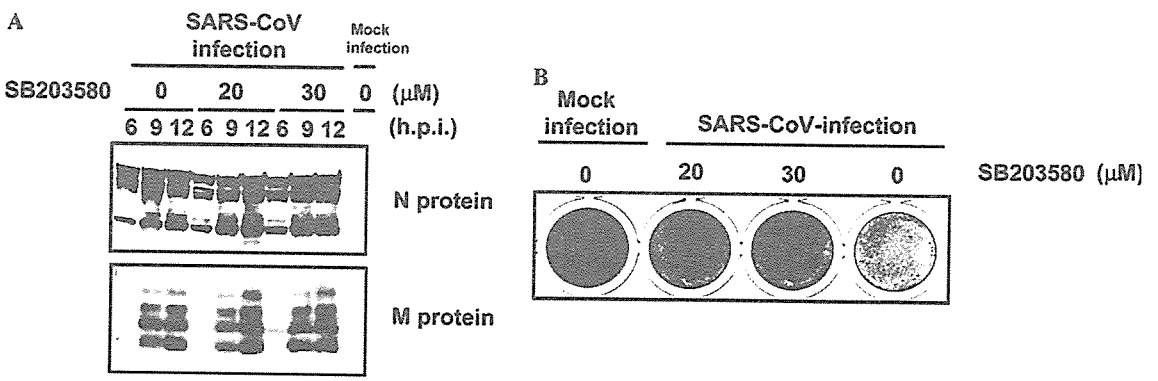

Fig. 8. Kinetics of N and M proteins synthesis in the presence of SB203580. After viral adsorption for 1 h, 20 and 30 μM of SB203580 was added to the cells. (A) Western blot analysis was performed at 6, 9, and 12 h.p.i. for detection of SARS-CoV N and M proteins. (B) Vero E6 cells were stained with 0.05% crystal violet at 41 h.p.i.

p38 MAPK is able to promote both cell death and survival [33], the substrates examined in this study and the other substrates of p38 MAPK may also induce cell death. Further studies are needed to determine which target molecules of p38 MAPK have inductive and preventative effects on apoptosis. To our knowledge, this is the first demonstration of activation of signaling transduction due to SARS-CoV-infection.

Acknowledgments

We thank Drs. F. Taguchi (National Institute of Infectious Diseases, Japan) for useful suggestions. We also thank Ms. M. Ogata (National Institute of Infectious Diseases, Japan) for her assistance. This work is partly supported by a grant-in-aid from the Ministry of Health, Labor and Welfare of Japan and Japan Health Science Foundation, Tokyo, Japan.

References

[1] P.A. Rota, M.S. Oberste, S.S. Monroe, W.A. Nix, R. Campagnoli, J.P. Icenogle, S. Penaranda, B. Bankamp, K. Maher, M.H. Chen, S. Tong, A. Tamin, L. Lowe, M. Frace, J.L. DeRisi, Q. Chen, D. Wang, D.D. Erdman, T.C. Peret, C. Burns, T.G. Ksiazek, P.E. Rollin, A. Sanchez, S. Liffick, B. Holloway, J. Limor, K. McCaustland, M. Olsen-Rasmussen, R. Fouchier, S. Gunther, A.D. Osterhaus, C. Drosten, M.A. Pallansch, L.J. Anderson, W.J. Bellini, Characterization of a novel coronavirus associated with severe acute respiratory syndrome, Science 300 (5624) (2003) 1394–1399.

[2] M.A. Marra, S.J. Jones, C.R. Astell, R.A. Holt, A. Brooks-Wilson, Y.S. Butterfield, J. Khattra, J.K. Asano, S.A. Barber, S.Y. Chan, A. Cloutier, S.M. Coughlin, D. Freeman, N. Girn, O.L. Griffith, S.R. Leach, M. Mayo, H. McDonald, S.B. Montgomery, P.K. Pandoh, A.S. Petrescu, A.G. Robertson, J.E. Schein, A. Siddiqui, D.E. Smailus, J.M. Stott, G.S. Yang, F. Plummer, A. Andonov, H. Artsob, N. Bastien, K. Bernard, T.F. Booth, D. Bowness, M. Czub, M. Drebot, L. Fernando, R. Flick, M. Garbutt, M. Gray, A. Grolla, S. Jones, H. Feldmann, A. Meyers, A. Kabani, Y. Li, S. Normand, U. Stroher, G.A. Tipples, S. Tyler, R. Vogrig, D. Ward, B. Watson, R.C. Brunham, M. Krajden, M. Petric, D.M. Skowronski, C. Upton, R.L. Roper, The genome sequence of the SARS-associated coronavirus, Science 300 (5624) (2003) 1399–1404.

[3] T.P. Garrington, G.L. Johnson, Organization and regulation of mitogen-activated protein kinase signaling pathways, Curr. Opin. Cell. Biol. 11 (1999) 211–218.

[4] A.J. Whitmarsh, R.J. Davis, A central control for cell growth, Nature 403 (2000) 255–256.

[5] L. Chang, M. Karin, Mammalian MAP kinase signalling cascades, Nature 410 (6824) (2001) 37–40.

[6] J.M. Kyriakis, J. Avruch, Mammalian mitogen-activated protein kinase signal transduction pathways activated by stress and inflammation, Physiol. Rev. 81 (2001) 807–869.

[7] S. Banerjee, K. Narayanan, T. Mizutani, S. Makino, Murine coronavirus replication-induced p38 mitogen-activated protein kinase activation promotes interleukin-6 production and virus replication in cultured cells, J. Virol. 76 (2002) 5937–5948.

[8] R. He, A. Leeson, A. Andonov, Y. Li, N. Bastien, J. Cao, C. Osiowy, F. Dobie, T. Cutts, M. Ballantine, X. Li, Activation of AP-1 signal transduction pathway by SARS coronavirus nucleocapsid protein, Biochem. Biophys. Res. Commun. 311 (2003) 870–876.

[9] C. Drosten, S. Gunther, W. Preiser, S. van der Werf, H.R. Brodt, S. Becker, H. Rabenau, M. Panning, L. Kolesnikova, R.A. Fouchier, A. Berger, A.M. Burguiere, J. Cinatl, M. Eickmann, N. Escriou, K. Grywna, S. Kramme, J.C. Manuguerra, S. Muller, V. Rickerts, M. Sturmer, S. Vieth, H.D. Klenk, A.D. Osterhaus, H. Schmitz, W. Doerr, Identification of a novel coronavirus in patients with severe acute respiratory syndrome, N. Engl. J. Med. 348 (20) (2003) 1967–1976.

[10] V. Thiel, K.A. Ivanov, A. Putics, T. Hertzig, B. Schelle, S. Bayer, B. Weissbrich, E.J. Snijder, H. Rabenau, H.W. Doerr, A.E. Gorbalenya, J. Ziebuhr, Mechanisms and enzymes involved in SARS coronavirus genome expression, J. Gen. Virol. 84 (2003) 2305–2315.

[11] T. Mizutani, M. Kobayashi, Y. Eshita, K. Shirato, T. Kimura, Y. Ako, H. Miyoshi, T. Takasaki, T. Kurane, H. Kariwa, T. Umemura, I. Takashima, Involvement of the JNK-like protein of the *Aedes albopictus* mosquito cell line, C6/36, in phagocytosis, endocytosis and infection of West Nile virus, Insect Mol. Biol. 12 (2003) 491–499.

[12] T.G. Ksiazek, D. Erdman, C.S. Goldsmith, S.R. Zaki, T. Peret, S. Emery, S. Tong, C. Urbani, J.A. Comer, W. Lim, P.E. Rollin, S.F. Dowell, A.E. Ling, C.D. Humphrey, W.J. Shieh, J. Guarner, C.D. Paddock, P. Rota, B. Fields, J. DeRisi, J.Y. Yang, N. Cox, J.M. Hughes, J.W. LeDuc, W.J. Bellini, L.J. Anderson, SARS working group. A novel coronavirus associated with severe acute respiratory syndrome, N. Engl. J. Med. 348 (20) (2003) 1953–1966.

[13] C.J. Chen, S. Makino, Murine coronavirus-induced apoptosis in 17Cl-1 cells involves a mitochondria-mediated pathway and its downstream caspase-8 activation and bid cleavage, Virology 302 (2002) 321–332.

[14] C. Liu, H.Y. Xu, D.X. Liu, Induction of caspase-dependent apoptosis in cultured cells by the avian coronavirus infectious bronchitis virus, J. Virol. 75 (2001) 6402–6409.

[15] M.S. Iordanov, J.M. Paranjape, A. Zhou, J. Wong, B.R. Williams, E.F. Meurs, R.H. Silverman, B.E. Magun, Activation of p38 mitogen-activated protein kinase and c-Jun NH_2-terminal kinase by double-stranded RNA and encephalomyocarditis virus: involvement of RNase L, protein kinase R, and alternative pathways, Mol. Cell. Biol. 20 (2000) 617–627.

[16] N. Juretic, J.F. Santibanez, C. Hurtado, J. Martinez, ERK 1,2 and p38 pathways are involved in the proliferative stimuli mediated by urokinase in osteoblastic SaOS-2 cell line, J. Cell. Biochem. 83 (2001) 92–98.

[17] B. Liu, M. Fang, Y. Lu, G.B. Mills, Z. Fan, Involvement of JNK-mediated pathway in EGF-mediated protection against paclitaxel-induced apoptosis in SiHa human cervical cancer cells, Br. J. Cancer 85 (2001) 303–311.

[18] G. Yosimichi, T. Nakanishi, T. Nishida, T. Hattori, T. Takano-Yamamoto, M. Takigawa, CTGF/Hcs24 induces chondrocyte differentiation through a p38 mitogen-activated protein kinase (p38MAPK), and proliferation through a p44/42 MAPK/extracellular-signal regulated kinase (ERK), Eur. J. Biochem. 268 (2001) 6058–6065.

[19] I.N. Foltz, J.C. Lee, P.R. Young, J.W. Schrader, Hemopoietic growth factors with the exception of interleukin-4 activate the p38 mitogen-activated protein kinase pathway, J. Biol. Chem. 272 (1997) 3296–3301.

[20] N.W. Freshney, L. Rawlinson, F. Guesdon, E. Jones, S. Cowley, J. Hsuan, J. Saklatvala, Interleukin-1 activates a novel protein kinase cascade that results in the phosphorylation of Hsp27, Cell 78 (1994) 1039–1049.

[21] C. Garrido, E. Schmitt, C. Cande, N. Vahsen, A. Parcellier, G. Kroemer, HSP27 and HSP70: potentially oncogenic apoptosis inhibitors, Cell Cycle 2 (2003) 579–584.

[22] Y. Tan, J. Rouse, A. Zhang, S. Cariati, P. Cohen, M.J. Comb, FGF and stress regulate CREB and ATF-1 via a pathway involving p38 MAP kinase and MAPKAP kinase-2, EMBO J. 15 (1996) 4629–4642.
[23] D.D. Ginty, A. Bonni, M.E. Greenberg, Nerve growth factor activates a Ras-dependent protein kinase that stimulates c-fos transcription via phosphorylation of CREB, Cell 77 (1994) 713–725.
[24] A. von Knethen, A. Lotero, B. Brune, Etoposide and cisplatin induced apoptosis in activated RAW 264.7 macrophages is attenuated by cAMP-induced gene expression, Oncogene 17 (1998) 387–394.
[25] S. Pugazhenthi, T. Boras, D. O'Connor, M.K. Meintzer, K.A. Heidenreich, J.E. Reusch, Insulin-like growth factor I-mediated activation of the transcription factor cAMP response element-binding protein in PC12 cells. Involvement of p38 mitogen-activated protein kinase-mediated pathway, J. Biol. Chem. 274 (1999) 2829–2837.
[26] M. Parrizas, D. LeRoith, Specific inhibition of insulin-like growth factor-1 and insulin receptor tyrosine kinase activity and biological function by tyrphostins, Endocrinology 138 (1997) 1355–1358.
[27] K.A. Lee, N. Masson, Transcriptional regulation by CREB and its relatives, Biochim. Biophys. Acta 1174 (1993) 221–233.
[28] D. Jean, M. Harbison, D.J. McConkey, Z. Ronai, M. Bar-Eli, CREB and its associated proteins act as survival factors for human melanoma cells, J. Biol. Chem. 273 (1998) 24884–24890.
[29] S.J. Morley, L. McKendrick, Involvement of stress-activated protein kinase and p38/RK mitogen-activated protein kinase signaling pathways in the enhanced phosphorylation of initiation factor 4E in NIH 3T3 cells, J. Biol. Chem. 272 (1997) 17887–17893.
[30] S. Pyronnet, H. Imataka, A.C. Gingras, R. Fukunaga, T. Hunter, N. Sonenberg, Human eukaryotic translation initiation factor 4G (eIF4G) recruits mnk1 to phosphorylate eIF4E, EMBO J. 18 (1999) 270–279.
[31] A.C. Gingras, B. Raught, N. Sonenberg, eIF4 initiation factors: effectors of mRNA recruitment to ribosomes and regulators of translation, Annu. Rev. Biochem. 68 (1999) 913–963.
[32] A. Cuenda, D.R. Alessi, Use of kinase inhibitors to dissect signaling pathways, Methods Mol. Biol. 99 (2000) 161–175.
[33] P. Dent, A. Yacoub, P.B. Fisher, P.M.P. Hagan, S. Grant, MAPK pathways in radiation responses, Oncogene 22 (2003) 5885–5896.

Available online at www.sciencedirect.com

SCIENCE DIRECT®

Virology 327 (2004) 169–174

VIROLOGY

www.elsevier.com/locate/yviro

Rapid Communication

Importance of Akt signaling pathway for apoptosis in SARS-CoV-infected Vero E6 cells

Tetsuya Mizutani*, Shuetsu Fukushi, Masayuki Saijo, Ichiro Kurane, Shigeru Morikawa

Special Pathogens Laboratory, Department of Virology 1, National Institute of Infectious Diseases, Musashimurayama, Tokyo 208-0011, Japan

Received 26 May 2004; accepted 9 July 2004

Abstract

Severe acute respiratory syndrome (SARS) is an acute respiratory tract infectious disease that is associated with a new coronavirus (SARS-CoV). Our recent study indicated that SARS-CoV infection induces activation of the p38 mitogen-activated protein kinase (MAPK) signaling pathway and the p38 MAPK inhibitor partially inhibited its cytopathic effect in Vero E6 cells. The results of the present study indicated that before cell death, Akt, which is an inhibitor of apoptosis, was also activated in response to viral replication. Phosphorylation of a serine residue on Akt was detected at least 8 h postinfection (hpi), which declined after 18 hpi. Thus, the phosphatidylinositol 3-kinase (PI3K)/Akt pathway is activated in virus-infected Vero E6 cells. However, a threonine residue was not phosphorylated. A downstream target of Akt, glycogen synthase kinase 3β (GSK-3β), was slightly phosphorylated, indicating that the level of activation of Akt was very low. PKCζ, which is downstream of the PI3K pathway, was also phosphorylated in virus-infected cells. These results suggested that weak activation of Akt cannot prevent apoptosis induced by SARS-CoV infection in Vero E6 cells.

Keywords: SARS-CoV; Akt; PI3K; PKC

Severe acute respiratory syndrome (SARS) is a newly described infectious disease caused by a coronavirus (Rota et al., 2003). Although the mechanism of SARS pathogenesis in vivo may involve both the effect of viral replication in target cells and immune responses, there is a lack of molecular pathological data including signaling pathways of SARS-coronavirus (CoV) infection. Recently, we reported that infection with SARS-CoV caused apoptosis in Vero E6 cells and that p38 mitogen-activated protein kinase (MAPK) was activated during infection (Mizutani et al., 2004). Thus, it is important to investigate the apoptotic events that occur in SARS-CoV-infected cells to understand the pathogenesis of SARS-CoV. Generally, both pro-apoptotic and pro-survival signaling pathways are activated after apoptotic signaling, and there are many pro- and anti-apoptotic proteins involved in these pathways in cells. The present study was performed to clarify the activated signaling pathways related to apoptotic events in SARS-CoV-infected Vero E6 cells.

In SARS-CoV-infected Vero E6 cells, cytopathic effects were observed within 24 h postinfection (hpi). We have recently shown that p38 MAPK and its downstream targets are phosphorylated in SARS-CoV-infected Vero E6 cells (Mizutani et al., 2004). These findings suggest that other signaling pathways are also activated in SARS-CoV-infected cells. To investigate such cellular responses in SARS-CoV-infected Vero E6 cells before apoptosis, proteins of SARS-CoV-infected and mock-infected cells were analyzed by Western blotting analysis at 18 hpi using 125 antibodies to human cellular proteins. We found that antibodies to proteins related to several signaling pathways responded specifically in SARS-CoV infection (\ below and unpublished data).

One such signaling pathway, protein kinase B (PKB), known as Akt, has been studied intensively (Toker, 2000;

* Corresponding author. Special Pathogens Laboratory, Department of Virology 1, National Institute of Infectious Diseases, Gakuen 4-7-1, Musashimurayama, Tokyo 208-0011, Japan. Fax: +81 42 564 4881.
E-mail address: tmizutan@nih.go.jp (T. Mizutani).

0042-6822/$ - see front matter © 2004 Elsevier Inc. All rights reserved.
doi:10.1016/j.virol.2004.07.005

Brazil and Hemmings, 2001; Scheid and Woodgett, 2003). Akt is phosphorylated at both serine 473 and threonine 308 residues through a phosphatidylinositol 3-kinase (PI3K)-dependent mechanism on stimulation by growth factors, insulin, and hormones (Welch et al., 1998). An important function of activated Akt in cells is inhibition of apoptosis. Downstream targets of Akt induce cell survival via phosphorylation of the forkhead transcription factor (FKHR) family, glycogen synthase kinase 3β (GSK-3β), caspase-9, and Bad (Cardone et al., 1998; Cross et al., 1995; Datta et al., 1997). To examine the phosphorylation of Akt in virus-infected cells, Western blotting analysis was performed using anti-phospho Akt antibodies. As shown in Fig. 1A, serine 473 of Akt was phosphorylated at 8 hpi by SARS-CoV. The phosphorylated serine 473 of Akt began to accumulate at least 8 hpi and maximal phosphorylation was observed at 18 hpi. Western blotting analysis with a phosphorylation-state-independent anti-Akt antibody revealed the presence of Akt in Vero E6 cells, whereas a threonine 308 phosphorylation-state-dependent antibody failed to demonstrate the presence of threonine 308 phosphorylated Akt in virus-infected cells (Fig. 1A). In addition, serine phosphorylation was dependent on SARS-CoV infection into Vero E6 cells, because the UV-inactivated virus failed to induce serine phosphorylation. Brief stimulation by epidermal growth factor (EGF) also showed only serine 473 phosphorylation of Akt (Fig. 1B), suggesting that threonine 308 of Akt is difficult to phosphorylate in Vero E6 cells. Therefore, total activity of Akt may be low in Vero E6 cells. However, it is possible that the anti-phospho Akt (threonine 308) antibody used in the present study is unable to recognize threonine phosphorylation of Akt in Vero E6 cells as the datasheet included no description of cross-reactivity with monkey. To investigate whether SARS-CoV-induced Akt serine phosphorylation represented a biologically active kinase, we examined the in vitro kinase activity of phosphorylated Akt in SARS-CoV-infected cells. The SARS-CoV-infected Vero E6 cells were lysed at 18 hpi and serine 473-phosphorylated Akt in the cell lysate was precipitated by anti-serine 473-phosphorylated Akt antibody. GSK-3β protein was added to the immunoprecipitated phosphorylated Akt with ATP, and Western blotting was performed using anti-phosphorylated GSK-3α/β (Ser21/9) antibody. As shown in Fig. 1C, immunoprecipitated Akt was almost at the same amount between SARS-CoV-infected cells and mock-infected cells at 18 hpi. The amount of serine 473-phosphorylated Akt in SARS-CoV-infected cells was higher than that in mock-infected controls. The level of phosphorylation of GSK-3α/β in virus-infected cells was slightly higher than that in mock-infected controls. These results strongly suggested that Akt in Vero E6 cells was phosphorylated only at serine residues by SARS-CoV infection, but the level of activity of Akt was low.

To investigate phosphorylation of up- and downstream targets of Akt in virus-infected cells, Western blotting analysis was performed. Of the Akt targets mentioned above, the level of phosphorylation of GSK-3β (Ser9) was slightly increased, while phosphorylated Bad and FKHR were not detected (Fig. 1C). GSK-3 β is a pro-apoptotic signaling molecule and is inactivated by phosphorylation of the N-terminal serine residue Ser9 (Pap and Cooper, 1998).

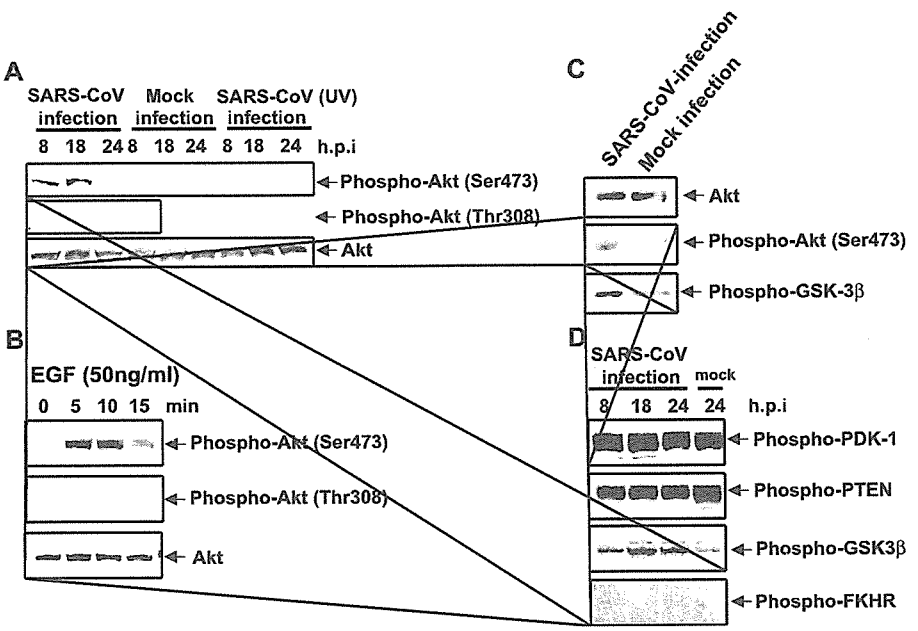

Fig. 1. Phosphorylation of Akt in SARS-CoV-infected Vero E6 cells. (A) Vero E6 cells were infected with SARS-CoV at moi of 5, and Western blotting was then performed using proteins obtained at 8, 18, and 24 hpi. FCS-free medium and UV-inactivated SARS-CoV were used as controls. Phosphorylated Akt was detected by Western blotting analysis. (B) EGF was added to Vero E6 cells for 5, 10, and 15 min. (C) In vitro Akt kinase assay was performed using proteins from SARS-CoV-infected Vero E6 cells and mock-infected cells at 18 hpi. (D) Phosphorylation of up- and downstream targets of Akt was detected by Western blotting analysis.

Therefore, these results suggested that the phosphorylation of Akt in Vero E6 cells results in a low level of anti-apoptotic response to SARS-CoV infection. Recent studies explained the activation cycle of Akt as outlined below (Toker, 2000; Brazil and Hemmings, 2001; Scheid and Woodgett, 2003). Activation of PI3K results in local accumulation of phosphatidylinositol (PtdIns)-3,4,5-triphosphate (P3) at the plasma membrane, and PTEN phosphatase inhibits PI3K signaling. Cytosolic Akt is inactive and the activity of cytosolic PDK-1 is low. PtdIns-3,4,5-P3 recruits PDK-1 and Akt to the plasma membrane, and then Akt is autophosphorylated at serine 473. After PDK-1 activation on the plasma membrane, PDK-1 phosphorylates Akt on threonine 308, and then Akt shows a high level of activity. Thus, activation of upstream kinases of Akt is important for the activation of Akt. Fig. 1C shows that the amounts of both phosphorylated PTEN and PDK-1 were not significantly altered in SARS-CoV-infected Vero E6 cells. Therefore, these results may explain why no increase in threonine 308 phosphorylation of Akt was observed on virus infection.

The PI3 kinase inhibitor LY294002 is widely used to study Akt phosphorylation in stimulations in vitro. We examined whether LY294002 inhibits serine phosphorylation of Akt induced by SARS-CoV infection. Vero E6 cells were treated with LY294002 (10 and 20 μM) for 1.5 h, and then infected with SARS-CoV. Western blotting analysis was performed on the cell lysate at 18 hpi. As shown in Fig. 2A, the serine residue of Akt was not phosphorylated in cells treated with either concentration of LY294002. This result suggested that serine phosphorylation of Akt was sensitive to the PI3K inhibitor and that PI3K was activated in virus-infected cells. In addition, DNA fragmentations in infected Vero E6 cells at 30 hpi were similar in the presence and absence of LY294002 (Fig. 2B), suggesting that weak activation of Akt cannot prevent apoptosis induced by SARS-CoV infection in Vero E6 cells.

As shown in Fig. 2A, the level of viral N protein expression seemed to be similar at 18 hpi among cells treated with various amounts of LY294002. Next, we investigated whether enhancement of virus-specific protein synthesis through Akt-serine 473 phosphorylation occurs in SARS-CoV-infected cells at early time points pi. Recently, Simmons et al. (2004) reported that acidification of endosomes was required for SARS-CoV S-mediated viral entry using S glycoprotein pseudoviruses, after viral adsorption to angiotensin-converting enzyme (ACE)2 (Li et al., 2003). They reported that SARS-CoV S protein is cleaved in the presence of trypsin and that the cleaved S induces cell fusion. Their results suggested that SARS-CoV enters cells via endocytosis. Before a virus infection experiment, to verify that LY294002 has no effect on acidification of intracellular compartments in Vero E6 cells, LY294002 was added to the cells, followed by staining with acridine orange to detect intracellular acidic compartments (Mizutani et al., 2003). As indicated in Fig. 2C, neither 10 nor 20 μM LY294002 had any effect on the acidification of intracellular compartments, suggesting that treatment with LY294002 did not inhibit endocytosis in Vero E6 cells. Next, Western blotting analysis was performed at 6, 9, and 12 hpi using anti-N antibody. As shown in Fig. 2D, the kinetics of SARS-CoV-N protein accumulation in infected Vero E6 cells were similar in the presence and absence of LY294002. These

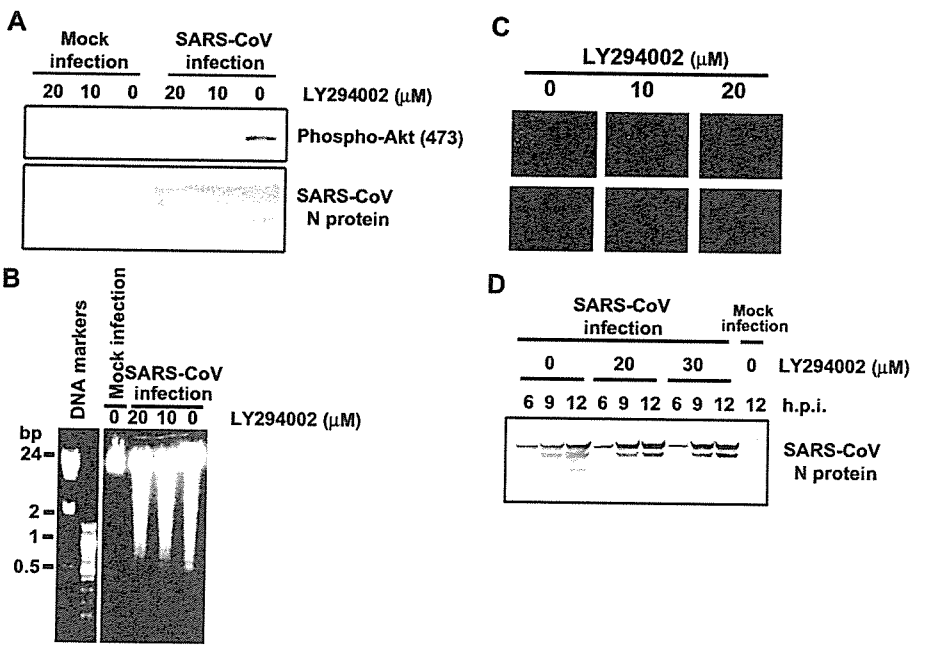

Fig. 2. Effects of LY294002 on SARS-CoV infection. (A) Vero E6 cells were pretreated with LY294002 and then infected with SARS-CoV at moi of 5. Western blotting analysis was performed at 18 hpi. (B) Cellular DNA was extracted from Vero E6 cells in the presence or absence of LY294002 at 30 hpi. (C) Vero E6 cells were incubated for 1.5 h with LY294002 and stained with acridine orange. (D) Western blotting analysis was performed at 6, 9, and 12 hpi for detection of SARS-CoV N protein.

results indicated that Akt serine phosphorylation induced by SARS-CoV infection had no effect on viral replication.

Protein kinase C (PKC) is also a major cellular mediator of biological functions. The PKC superfamily is divided into sub-superfamilies according to their activation profiles; conventional PKC (cPKC α, βI, βII, γ novel PKC (nPKC δ, ε, η, θ), atypical PKC (aPKCζ, ι/λ), PKCμ/PKD, and PKCυ (Toker, 2000). PKCζ was originally discovered as a unique PKC isotype (Ono et al., 1989). B cell survival by nerve growth factor (NGF) is mediated by PI3K-dependent activation of PKCζ (Kronfeld et al., 2002) and Akt could interact with PKCζ (Konishi et al., 1994). To determine if PKCζ is phosphorylated by SARS-CoV infection, Western blotting analysis was performed using an anti-phospho PKCζ (Thr410) antibody. As shown in Fig. 3, PKCζ was phosphorylated at 8 hpi, suggesting that PKCζ is activated as an anti-apoptotic response to virus infection. The antibody used in the present study can also detect phosphorylated PKCλ, and the function of PKCζ is still not clear. A novel PKC subfamily PKCθ was also very slightly phosphorylated by virus infection. In addition, PKCα/βII and δ (Ser643) were always phosphorylated in both virus-infected and mock-infected cells. These results suggested that the interaction of phosphorylation of PKCζ with Akt plays an important role in protection against SARS-CoV infection (Fig. 4).

In the present study, we showed that the PI3K/Akt pathway including PKCζ is activated by SARS-CoV infection, but that the level of activation of Akt in infected cells is very low. In virus infection, two conflicting cellular programs are triggered in cells: apoptosis to eliminate virus-infected cells and cell survival delaying cell death to alert naive cells by producing antiviral cytokines. This raises the question of how cell survival or death of SARS-CoV-infected cells is determined. The control mechanisms that balance cell survival against cell death are not well understood.

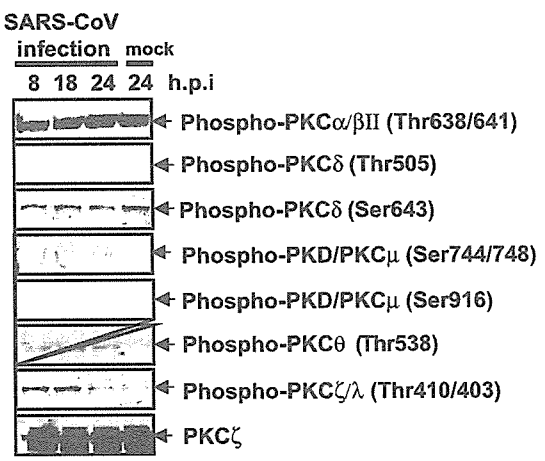

Fig. 3. Phosphorylation of PKCs in SARS-CoV-infected Vero E6 cells. Phosphorylated PKCs were detected by Western blotting analysis using proteins isolated from SARS-CoV-infected Vero E6 cells at 8, 18, and 24 hpi.

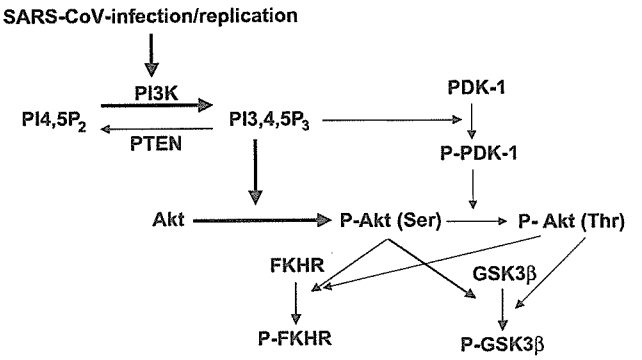

Fig. 4. Phosphorylation of Akt/PI3K signaling pathway in SARS-CoV-infected Vero E6 cells. Bold lines indicate activated pathways in viral-infected cells. Week or no activated pathways are indicated by thin lines.

Previously, we showed that activation of the p38 MAPK signaling pathway induced by SARS-CoV infection has a partially pro-apoptotic role in Vero E6 cells (Mizutani et al., 2004). The role of p38 MAPK signaling in cellular responses is diverse depending on the cell type and stimulus. For example, p38 MAPK signaling has been shown to promote cell death as well as to enhance cell growth and survival (Juretic et al., 2001; Liu et al., 2001; Yosimichi et al., 2001). In virus-infected Vero E6 cells, CREB and HSP-27, which have anti-apoptotic roles, were shown to be phosphorylated (Mizutani et al., 2004). Therefore, pro-apoptotic molecules downstream of targets of p38 MAPK may exist in Vero E6 cells. On the other hand, Akt, which is a key regulator of cell survival events, targets several different cytoplasmic proteins, including pro-apoptotic molecules, such as GSK3β, caspase-9, Bad, and FKHR. Phosphorylation of these proteins by Akt generally results in their inactivation and inability to activate pro-apoptotic pathways. In the present study, phosphorylation of GSK3β serine 9 was found in virus-infected cells. However, our results suggested that the level of phosphorylation of GSK3β is not sufficient to prevent apoptosis.

In conclusion, incomplete activation of Akt induces apoptosis in SARS-CoV-infected Vero E6 cells. However, we cannot exclude the possibility of the involvement of other signaling pathways that strongly induce apoptosis. These findings may facilitate the development of a new way to block apoptosis upstream and help in the development of anti-SARS-CoV agents.

Materials and methods

Cells and virus

Vero E6 cells were routinely subcultured in 75-cm^3 flasks in Dulbecco's modified Eagle's medium (DMEM, Sigma, St. Louis, MO, USA) supplemented with 0.2 mM L-glutamine, 100 units/ml penicillin, 100 μg/ml streptomycin, and 5% (v/v) fetal bovine serum (FBS), and maintained at

37 °C in an atmosphere of 5% CO_2. For use in the experiments, the cells were split once they reached 90% confluence and seeded onto 6- or 24-well tissue culture plate inserts. The culture medium was changed to 2% FBS containing DMEM before virus infection. In the present study, we used SARS-CoV (Drosten et al., 2003), which was isolated as Frankfurt 1 (Thiel et al., 2003) and kindly provided by Dr. J. Ziebuhr. Infection was usually performed with a multiplicity of infection (moi) of 5.

Western blotting

After virus infection, whole-cell extracts were electrophoresed in 12.5% and 10–20% gradient polyacrylamide gels, and transferred onto PVDF membranes (Immobilon-P, Millipore, Bedford, MA, USA). We applied two sets of samples to polyacrylamide gels, and the blots were divided into two sheets. The following antibodies were used at a dilution of 1:1000 (Cell Signaling Technology Inc., Beverly, MA, USA): Rabbit anti-phospho Akt (Ser473), rabbit anti-phospho Akt (Thr308), rabbit anti-Akt, rabbit anti-phospho GSK-3β (Ser9), anti-phospho FKHR (Ser256), anti-phospho PTEN (Ser380), rabbit anti-phospho PDK-1, rabbit Phospho-PKCα/βII (Thr638/641) antibody, rabbit anti-phospho-PKCδ (Thr505) antibody, rabbit anti-phospho-PKCδ (Ser643) antibody, rabbit anti-phospho-PKD/PKCμ (Ser744/748) antibody, rabbit anti-phospho-PKD/PKCμ (Ser916) antibody, rabbit anti-phospho-PKCζ (Thr538) antibody, and rabbit anti-phospho-PKCζ/λ (Thr410/403) antibody. Rabbit anti-PKCζ antibody (diluted 1:1000) was purchased from Santa Cruz Biotechnology (Santa Cruz, CA, USA). Rabbit anti-SARS N and M antibodies were described previously (Mizutani, 2004). After 15-h incubation, the membrane was washed with 0.1% TBS-Tween and specific proteins were detected with a ProtoBlot II AP system (Promega Co., Madison, WI, USA), as described previously (Mizutani et al., 2003).

In vitro GSK-3 activation assay

Vero E6 cells were infected with SARS-CoV at moi of 10 for 18 hpi, and then cell extracts were obtained using the lysis buffer supplied with the Akt kinase assay kit (Cell Signaling Technology Inc., Bedford, MA, USA). Selective immunoprecipitation of Akt was performed using immobilized Akt (serine phosphorylation) antibody. After incubation of immunoprecipitated Akt in kinase buffer containing GSK-3β fusion protein and ATP, GSK-3α/β (Ser21/9) phosphorylation was analyzed by Western blotting using anti-phospho GSK-3 antibody.

DNA fragmentation

Vero E6 cells were pretreated with LY294002 for 1.5 h, and then 5 moi of SARS-CoV was inoculated. At 30 hpi, DNA was extracted using MEBCYTO Apoptosis ladder detection kit (Medical and Biological Laboratories, Co. LTD., Nagoya, Japan), as described previously (Mizutani et al., 2004). The DNA was analyzed by electrophoresis on 1% agarose gels and then stained with ethidium bromide.

Endocytosis assay

Vero E6 cells at 50% confluency in 24-well plates were incubated for 1.5 h with 10 or 20 μM LY294002 (Cell Signaling Technology Inc.) or dimethyl sulfoxide (DMSO) in 1 ml of medium. The LY294002 was dissolved in DMSO. The medium was removed and 5 μg/ml of acridine orange (Wako, Osaka, Japan) in Mg^{2+}-free Hank's solution was added to the cells. After incubation for 5 min, the cells were washed twice with Hank's solution, followed by addition of 0.5% trypan blue solution. Fluorescence micrographs were taken at the same shutter speed for each experiment.

Acknowledgments

We thank Dr. F. Taguchi (National Institute of Infectious Diseases, Japan) for useful suggestions. We also thank Ms. M. Ogata (National Institute of Infectious Diseases, Japan) for her assistance. This work was supported in part by a grant-in-aid from the Ministry of Health, Labor, and Welfare of Japan and the Japan Health Science Foundation, Tokyo, Japan.

References

Brazil, D.P., Hemmings, B.A., 2001. Ten years of protein kinase B signalling: a hard Akt to follow. Trends Biochem. Sci. 26, 657–664.

Cardone, M.H., Roy, N., Stennicke, H.R., Salvesen, G.S., Franke, T.F., Stanbridge, E., Frisch, S., Reed, J.C., 1998. Regulation of cell death protease caspase-9 by phosphorylation. Science 282, 1318–1321.

Cross, D.A., Alessi, D.R., Cohen, P., Andjelkovich, M., Hemmings, B.A., 1995. Inhibition of glycogen synthase kinase-3 by insulin mediated by protein kinase B. Nature 378, 785–789.

Datta, S.R., Dudek, H., Tao, X., Masters, S., Fu, H., Gotoh, Y., Greenberg, M.E., 1997. Akt phosphorylation of BAD couples survival signals to the cell-intrinsic death machinery. Cell 91, 231–241.

Drosten, C., Gunther, S., Preiser, W., et al., 2003. Identification of a novel coronavirus in patients with severe acute respiratory syndrome. N. Engl. J. Med. 348, 1967–1976.

Juretic, N., Santibanez, J.F., Hurtado, C., Martinez, J., 2001. ERK 1,2 and p38 pathways are involved in the proliferative stimuli mediated by urokinase in osteoblastic SaOS-2 cell line. J. Cell. Biochem. 83, 92–98.

Konishi, H., Shinomura, T., Kuroda, S., Ono, Y., Kikkawa, U., 1994. Molecular cloning of rat RAC protein kinase alpha and beta and their association with protein kinase C zeta. Biochem. Biophys. Res. Commun. 205, 817–825.

Kronfeld, I., Kazimirsky, G., Gelfand, E.W., Brodie, C., 2002. NGF rescues human B lymphocytes from anti-IgM induced apoptosis by activation of PKC. Eur. J. Immunol. 32, 136–143.

Li, W., Moore, M.J., Vasilieva, N., Sui, J., Wong, S.K., Berne, M.A., Somasundaran, M., Sullivan, J.L., Luzuriaga, K., Greenough, T.C., Choe, H., Farzan, M., 2003. Angiotensin-converting enzyme 2 is a functional receptor for the SARS coronavirus. Nature 426, 450–454.

Liu, B., Fang, M., Lu, Y., Lu, Y., Mills, G.B., Fan, Z., 2001. Involvement of JNK-mediated pathway in EGF-mediated protection against paclitaxel-induced apoptosis in SiHa human cervical cancer cells. Br. J. Cancer. 85, 303–311.

Mizutani, T., Kobayashi, M., Eshita, Y., Shirato, K., Kimura, T., Ako, Y., Miyoshi, H., Takasaki, T., Kurane, T., Kariwa, H., Umemura, T., Takashima, I., 2003. Involvement of the JNK-like protein of the Aedes albopictus mosquito cell line, C6/36, in phagocytosis, endocytosis and infection of West Nile virus. Insect. Mol. Biol. 12, 491–499.

Mizutani, T., Fukushi, S., Morikawa, S., Saijo, M., Kurane, I., 2004. Phosphorylation of p38 MAPK and its downstream targets in SARS coronavirus-infected cells. Biochem. Biophys. Res. Commun. 319, 1228–1234.

Ono, Y., Fujii, T., Ogita, K., Kikkawa, U., Igarashi, K., Nishizuka, Y., 1989. Protein kinase C-subspecies from brain: its structure, expression and properties. Proc. Natl. Acad. Sci. U.S.A. 86, 3099–3103.

Pap, M., Cooper, G.M., 1998. Role of glycogen synthase kinase-3 in the phosphatidylinositol 3-Kinase/Akt cell survival pathway. J. Biol. Chem. 273, 19929–19932.

Rota, P.A., Oberste, M.S., Monroe, S.S., et al., 2003. Characterization of a novel coronavirus associated with severe acute respiratory syndrome. Science 300, 1394–1399.

Scheid, M.P., Woodgett, J.R., 2003. Unravelling the activation mechanisms of protein kinase B/Akt. FEBS Lett. 546, 108–112.

Simmons, G., Reeves, J.D., Rennekamp, A.J., Amberg, S.M., Piefer, A.J., Bates, P., 2004. Characterization of severe acute respiratory syndrome-associated coronavirus (SARS-CoV) spike glycoprotein-mediated viral entry. Proc. Natl. Acad. Sci. U.S.A. 101, 4240–4245.

Thiel, V., Ivanov, K.A., Putics, A., Hertzig, T., Schelle, B., Bayer, S., Weissbrich, B., Snijder, E.J., Rabenau, H., Doerr, H.W., Gorbalenya, A.E., Ziebuhr, J., 2003. Mechanisms and enzymes involved in SARS coronavirus genome expression. J. Gen. Virol. 84, 2305–2315.

Toker, A., 2000. Protein kinases as mediators of phosphoinositide 3-kinase signaling. Mol. Pharmacol. 57, 652–658.

Welch, H., Eguinoa, A., Stephens, L.R., Hawkins, P.T., 1998. Protein kinase B and rac are activated in parallel within a phosphatidylinositide 3OH-kinase-controlled signaling pathway. J. Biol. Chem. 273, 11248–11256.

Yosimichi, G., Nakanishi, T., Nishida, T., Hattori, T., Takano-Yamamoto, T., Takigawa, M., 2001. CTGF/Hcs24 induces chondrocyte differentiation through a p38 mitogen-activated protein kinase (p38MAPK), and proliferation through a p44/42 MAPK/extracellular-signal regulated kinase (ERK). Eur. J. Biochem. 268, 6058–6065.

FEBS 28924

FEBS Letters 577 (2004) 187–192

Tyrosine dephosphorylation of STAT3 in SARS coronavirus-infected Vero E6 cells

Tetsuya Mizutani[a,*], Shuetsu Fukushi[a], Masaaki Murakami[b], Toshio Hirano[b], Masayuki Saijo[a], Ichiro Kurane[a], Shigeru Morikawa[a]

[a] *Special Pathogens Laboratory, Department of Virology 1, National Institute of Infectious Diseases, Gakuen 4-7-1, Musashimurayama, Tokyo 208-0011, Japan*

[b] *Department of Molecular Oncology, Graduate School of Medicine, Graduate School of Frontier Biosciences, Osaka University, Suita, Osaka, Japan*

Received 23 July 2004; revised 27 September 2004; accepted 4 October 2004

Available online 14 October 2004

Edited by Hans-Dieter Klenk

Abstract **Severe acute respiratory syndrome (SARS) has become a global public health emergency. p38 mitogen-activated protein kinase (MAPK) and its downstream targets are activated in SARS coronavirus (SARS-CoV)-infected Vero E6 cells and activation of p38 MAPK enhances the cytopathic effects of SARS-CoV infection. In addition, weak activation of Akt cannot prevent SARS-CoV infection-induced apoptosis in Vero E6 cells. In the present study, we demonstrated that signal transducer and activator of transcription (STAT) 3, which is constitutively phosphorylated at tyrosine (Tyr)-705 and slightly phosphorylated at serine (Ser)-727 in Vero E6 cells, was dephosphorylated at Tyr-705 on SARS-CoV infection. In addition to phosphorylation of p38 MAPK in virus-infected cells, other MAPKs, i.e., extracellular signal-regulated kinase (ERK) 1/2 and c-Jun N-terminal kinase (JNK), were phosphorylated. Although inhibitors of ERK1/2 and JNK (PD98059 and SP600125) had no effect on phosphorylation status of STAT3, inhibitors of p38 MAPK (SB203580 and SB202190) partially inhibited dephosphorylation of STAT3 at Tyr-705. Tyr-705-phosphorylated STAT3 was localized mainly in the nucleus in mock infected cells, whereas STAT3 disappeared from the nucleus in virus-infected cells. As STAT3 acts as an activator of transcription in the nucleus, these results suggest that STAT3 lacks its activity on transcription in SARS-CoV-infected Vero E6 cells.**

Keywords: Severe acute respiratory syndrome coronavirus; Signal transducer and activator of transcription 3; p38; Extracellular signal-regulated kinase 1/2; c-Jun N-terminal kinase

1. Introduction

Severe acute respiratory syndrome (SARS) is a newly found infectious disease caused by a novel coronavirus, SARS coronavirus (SARS-CoV) [1,2]. In late 2002, SARS-CoV spread from Guangdong Province in China to more than 30 countries. The pathogenesis of SARS in vivo may be mediated by both the effect of viral replication in the target cells and immune responses. Recently, we reported that p38 mitogen-activated protein kinase (MAPK) plays important roles in the cytopathic effects and apoptosis in SARS-CoV-infected cells [3]. Furthermore, weak activation of Akt cannot prevent apoptosis by SARS-CoV-infection [4]. Thus, it is necessary to examine the signaling pathways in SARS-CoV-infected cells in culture to understand the molecular mechanisms of its pathology in vivo.

MAPKs are signal transducers that respond to extracellular stimulation by cytokines, growth factors, viral infection, and stressors, and in turn regulate cell differentiation, proliferation, survival, and apoptosis [5–8]. p38 MAPK is strongly activated by stressors and inflammatory cytokines. Our previous study indicated that p38 MAPK phosphorylation in SARS-CoV-infected Vero E6 cells reached the maximal level at 18 h post-infection (h.p.i.) and cytopathic effects (CPEs) were observed from 24 h.p.i. [3]. The CPEs were partially prevented by treatment with the p38 MAPK inhibitor SB203580, strongly suggesting that the p38 MAPK signaling pathway is involved in the control of cell death in SARS-CoV-infected Vero E6 cells. On the other hand, signal transducer and activator of transcription (STAT) proteins are transcription factors that mediate cytokines and growth factors. Activation of all STAT proteins is induced by phosphorylation of a single tyrosine residue, leading to dimerization via an intermolecular SH2 phosphotyrosine interaction [9–12]. STAT3 is a major transcription factor activated in response to cytokines, such as interleukin-6 (IL-6) and IL-10. Inhibition of STAT3 signaling by dominant negative and antisense STAT3 inhibitors resulted in a decrease in cell viability and subsequent apoptosis [13–15]. Thus, STAT3 is thought to act as an anti-apoptotic transcription factor. Recent studies indicated that interactions between STATs and some viral proteins cause degradation of STATs in virus-infected cells. For example, V protein of measles virus forms complexes with STAT1, STAT2, and STAT3, and inhibits extracellular (IL-6) and intracellular (v-Src) STAT3-dependent signaling [16]. Thus, measles virus-induced degradation of STATs may provide a mechanism for virus-induced cytokine inhibition that links innate immune evasion to adaptive immune suppression.

In the present study, we found that STAT3, constitutively phosphorylated at tyrosine (Tyr)-705 and slightly phosphorylated at serine (Ser)-727 in Vero E6 cells, was dephosphorylated at Tyr-705 by activation of p38 MAPK on SARS-CoV infection. Lack of transcriptional activity of STAT3 by viral infection may decrease anti-apoptotic activity in the cells.

* Corresponding author. Fax: +81-42-564-4881.
E-mail address: tmizutan@nih.go.jp (T. Mizutani).

0014-5793/$22.00
doi:10.1016/j.febslet.2004.10.005

2. Materials and methods

2.1. Cells and virus

Vero E6 cells were routinely subcultured in 75-cm^3 flasks in Dulbecco's modified Eagle's medium (DMEM, Sigma, St. Louis, MO, USA) supplemented with 0.2 mM L-glutamine, 100 units/ml penicillin, 100 μg/ml streptomycin, and 5% (v/v) fetal bovine serum (FBS), and maintained at 37 °C in an atmosphere of 5% CO_2. For use in the experiments, the cells were split once onto 6- or 24-well tissue culture plate inserts and cultured until they reached 100% confluence. The culture medium was changed to 2% FBS containing DMEM prior to virus infection. SARS-CoV, which was isolated as Frankfurt 1 [17] and kindly provided by Dr. J. Ziebuhr, was used in the present study. Infection was usually performed with a multiplicity of infection (m.o.i.) of 10.

2.2. Treatment with inhibitors

SB203580 and SB202190 as p38 MAPK inhibitors, PD098059 as a MEK inhibitor and SP600125 as a JNK inhibitor were dissolved in dimethyl sulfoxide (DMSO) at a concentration of 10 or 20 mM. All reagents were purchased from Calbiochem (San Diego, CA, USA). All test wells, including mock treated controls, were treated with 0.25% DMSO (v/v). Vero E6 cells were inoculated with SARS-CoV at m.o.i. of 10 for 1 h and then cells were treated with inhibitors for 17 h.

2.3. Subcellular fractionation

SARS-CoV-infected or mock infected Vero E6 cells at 18 h.p.i. were subjected to subcellular fractionation using a Subcellular Proteome Extraction Kit (Calbiochem) according to the manufacturer's instructions. Each subcellular fraction was then analyzed by Western blotting.

2.4. Western blotting

After virus infection, whole-cell extracts were electrophoresed on either 12.5% or 10–20% gradient polyacrylamide gels and transferred onto PVDF membranes (Immobilon-P, Millipore, Bedford, MA, USA). In the present study, we applied two sets of samples to polyacrylamide gels and the membranes were divided into two halves after blotting. The following antibodies, obtained from Cell Signaling Technology Inc. (Beverly, MA, USA), were used in the present study at a dilution of 1:1000: rabbit anti-phospho STAT3 (Tyr-705) antibody, rabbit anti-phospho STAT3 (Ser-727) antibody, rabbit anti-p38 MAPK (Thr180/Tyr182) antibody, rabbit anti-p38 MAPK antibody, rabbit anti-phospho p44/42 MAPK (Thr202/Tyr204) (=ERK1/2) antibody, rabbit anti-p44/42 MAPK (=ERK1/2) antibody, rabbit anti-phospho SAPK/JNK (Thr183/Tyr185) antibody, anti-SAPK/JNK antibody, anti-phospho MEK1/2 (Ser217/221) antibody, anti-MEK1/2 antibody, anti-phospho SEK1/MKK4 (Thr261) antibody, anti-SEK1/MKK4 antibody, anti-phospho MKK7 (Ser271/Thr275) antibody, anti-MKK7 antibody, anti-phospho MKK3/MKK6 (Ser189/207) antibody, anti-MKK3 antibody, anti-phospho Jak1 (Tyr1022/1023) an- tibody, anti-phospho JAK2 (Tyr1007/1008) antibody, and anti-phospho Tyk2 (Tyr1054/1055) antibody. Mouse anti-STAT3 antibody (diluted 1:2500), mouse anti-JAK1 antibody (diluted 1:250), and mouse anti-Tyk2 antibody (diluted 1:1000), obtained from BD Biosciences, Franklin Lakes, NJ, USA, were also used. Rabbit anti-JAK2 antibody (C-20, diluted 1:200) was obtained from Santa Cruz Biotechnology (Santa Cruz, CA, USA). After 15-h incubation with the above antibodies, the membranes were washed with Tris-borate saline containing 0.1% Tween 20 (0.1% TBS–Tween) and the reactions were detected with a ProtoBlot II AP system (Promega Co., Madison, WI, USA), as described previously [18].

3. Results

3.1. Tyrosine dephosphorylation of STAT3 in SARS-CoV-infected cells

As described in our previous report, we compared the cellular protein profiles of SARS-CoV-infected (18 h.p.i. when apoptosis was not evident) and mock infected Vero E6 cells by Western blotting using 125 antibodies to investigate cellular responses to SARS-CoV-infection [3,4]. Cellular proteins related to several signaling pathways that responded specifically to SARS-CoV infection, including p38 MAPK and Akt, were found. In the present study, we examined whether signal transducer and activator of transcription 3 (STAT3) was dysregulated on infection with SARS-CoV, as reported for measles virus-infection [16]. Vero E6 cells were infected with SARS-CoV at m.o.i. of 10, and cellular proteins were harvested at 6, 12, 18, and 24 h.p.i. Western blotting analysis was performed using a series of anti-STAT3 antibodies that recognized total STAT3 or Tyr-705- or Ser-727-phosphorylated forms of STAT3. In Vero E6 cells, STAT3 was phosphorylated constitutively at Tyr-705, whereas Ser-727 was only slightly phosphorylated (Fig. 1; mock infection). Constitutive activation of STAT3 was observed in breast carcinoma cell lines [19]. Interestingly, Tyr-705-phosphorylated STAT3 was not detected after 18 h.p.i. in SARS-CoV-infected Vero E6 cells, even though the total amount of STAT3 did not change until 24 h.p.i. (Fig. 1). This result suggested that STAT3 Tyr-705 was dephosphorylated from 18 to 24 h.p.i. On the other hand, Ser-727-phosphorylated STAT3 was slightly increased at the same time points. Based on the hypothesis that tyrosine phosphorylation of STAT is necessary for its activation [9–12], these results suggest that the level of activation of STAT3 was decreased in SARS-CoV-infected Vero E6 cells. Thus, the mechanism of dysregulation of STAT3 by SARS-CoV is different from that by measles virus in which Measles virus V protein forms complexes with STATs resulting in degradation of STAT3.

3.2. Phosphorylation level of upstream kinases of STAT3

As a general explanation of signal transduction of STAT3, binding of IL-6 to the receptor induces dimerization of the common gp130 signal transduction subunit of the IL-6 family of cytokine receptors, and then Janus kinases (JAK1 and 2) and Tyk2 are phosphorylated at tyrosine residues through a conserved membrane-proximal binding domain [20]. The phosphorylated JAKs and Tyk2 create docking sites for STAT3. Dimeric STAT3 Tyr-phosphorylated by JAKs and Tyk2 migrates to the nucleus, where STAT3 activates transcription of specific genes. Thus, JAK1, JAK2, Tyk2, and STAT3 are phosphorylated in response to IL-6. To test the hypothesis that Tyr-705-dephosphorylation of STAT3 by SARS-CoV infection occurred due to a lack of signals from JAK1/2 and Tyk2, the phosphorylation status of these kinases was examined in virus-infected or mock infected Vero E6 cells. As shown in Fig. 2, JAK1, JAK2, and Tyk2 were phosphor-

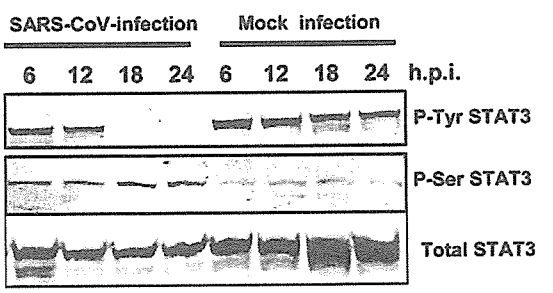

Fig. 1. Infection of Vero E6 cells with SARS-CoV affected the signaling pathway of STAT3. Western blotting analysis of proteins from SARS-CoV-infected Vero E6 cells was performed using antibodies that recognized forms of STAT3 phosphorylated at Tyr-705 or Ser-727.